AN IN-DEPTH STUDY OF ONE-SHOT OPTIMIZATION WITH APPLICATIONS TO MAGNETIC RESONANCE ELASTOGRAPHY

by

INGEBORG SAUGE TORPE

THESIS

for the degree of

MASTER OF SCIENCE

(Master i Anvendt matematikk og mekanikk)

Faculty of Mathematics and Natural Sciences
University of Oslo

June 2014

Det matematisk-naturvitenskapelige fakultet

Universitetet i Oslo

Abstract

The one-shot method is an approach to solve PDE-constrained optimization problems. In this thesis we study two models describing the deformation of biological tissue due to harmonic acoustic waves. These models are the Poisson equation and the linear elasticity model. By solving PDE-constrained optimization problems using the one-shot approach, the material parameters of tissue may be reconstructed. We study how Tikhonov regularization in the optimization problem affects the solution and the robustness of the method with noise in the target data. Numerical simulations are carried out using the finite element software FEniCS. Simulations are performed with both constructed data and later on with data from magnetic resonance elastography (MRE). The numerical results obtained in simulations with constructed data yielded qualitatively good results and were promising for this method to be used in application to MRE. However, carrying out simulations with MRE data, did not yield satisfactory solutions and thus changes of the model are necessary for further work.

Acknowledgment

First, I wish to express my gratitude to my two supervisors; Marie E. Rognes and Kent-Andre Mardal. Next, I would like to thank Karen-Helene Støverud, both for providing MRE data and for all helpful discussions along the way.

Further thanks go to my fellow students for good discussions and encouraging conversations.

Finally, I would like to thank my family and Erik for always believing in me and keeping my spirits up. I could not have done this without you!

Contents

Chapter 1

Introduction

The mechanical properties of biological tissue in the human body can tell us whether the tissue is healthy or not. Often the presence of stiffer (or harder) tissue is associated with pathological (non-healthy) tissue. For instance, most people have experienced going to the doctor for an examination, where the doctor uses his hands to feel after abnormalities. This technique is called palpation and is the oldest technique to find swellings, abnormal growth of tissue and so on. In the presence of stiffer tissue, this often represents an early warning sign for disease, because the tissue changes mechanical properties under pathological conditions [1; 2].

There exists several techniques to obtain mechanical properties of biological tissue. A review by Greenleaf et al. [3] discusses several methods for estimating the shear stiffness of tissue. Cheng et al. [4] offer a review of various techniques to obtain the material properties of the tissue in the brain and the spinal cord. Most of the techniques in use today are invasive and many are done in vitro. Therefore such data are commonly obtained from animals and not humans. Magnetic resonance elastography (MRE) is a non-invasive technique based on magnetic resonance imaging (MRI), which can be used to obtain information about mechanical properties of tissue in vivo. Mariappan et al. [2] present a review of the many applications and possibilities of elastography in medicine. By deciding the mechanical properties of tissue one can tell pathological tissue from healthy tissue. Among others, it can be used to diagnose liver diseases, breast or prostate cancer or fibrosis [2; 3].

In MRE acoustic waves are used to generate shear waves in tissue and MRI is used to image the propagation of the shear waves inside the tissue. The acoustic waves are typically at frequencies between 40 - 200 Hz [5]. The MRI images are processed to generate maps of the shear stiffness of the tissue, such maps are called elastograms. Figure 1.1 shows how shear waves propagate through a body and how an elastogram made from this MRE

looks; the left image shows a wave map of how the shear waves propagate through the medium, whereas the image to the right shows an elastogram of the medium with the values of the shear stiffness.

Elastography is already used in diagnosis of liver diseases. Today liver biopsy is the current standard for detecting liver fibrosis. This procedure is often painful and complications may occur [6]. Yin et al. [7] found in a study that elastography has very high effectiveness in distinguishing healthy livers from livers with fibrosis, with a negative predictive value of 97 %. Foucher et al. [8] have also proven elastography to be a safe way to diagnose cirrhosis. The technique of MRE is completely non-invasive, it does not use contrasts or ionising radiation, thus this technique is gentle on patients and there are no chance of complications.

A common method to compute the rheological parameters from elastography is direct inversion methods (see for instance [9]). This method reduces to a forward problem to solve for the shear modulus. However, according to [10] it suffers from following drawbacks:

1. the calculation of material parameters are based on differentiation of noisy measurements of the displacement field and the accuracy of the method is degraded due to performing this differentiation numerically, and

2. the required boundary data to create a well-posed forward problem for the shear modulus are not usually known.

On the other hand, in the one-shot optimization problem the solution is based on minimization the errors in the displacement field and shear modulus field compared to the measured target solutions, and the solutions are constrained to satisfy the equations of motion for harmonic displacement. Thus this method should in theory provide more accurate solutions than the method of direct inversion.

Biological tissue can be modelled in various ways, including as a purely elastic, as a poroelastic, or as a viscoelastic material. Given a model for the material, the material parameters and the applied forces, the deformation of biological tissue can be simulated using numerical methods. In this thesis we will study two models describing the deformation of biological tissue; the Poisson equation and the linear elasticity model. We will use PDE-constrained optimization and adjoint methods (one-shot approach) to solve minimization problems and study how Tikhonov regularization affects the solutions. Moreover, we will study how noise in measurement data affect the solutions of the optimization problems by using constructed data. Finally, we will perform simulations with real data from MRE measurements.

For the work of this thesis data from MRE examinations of the liver have

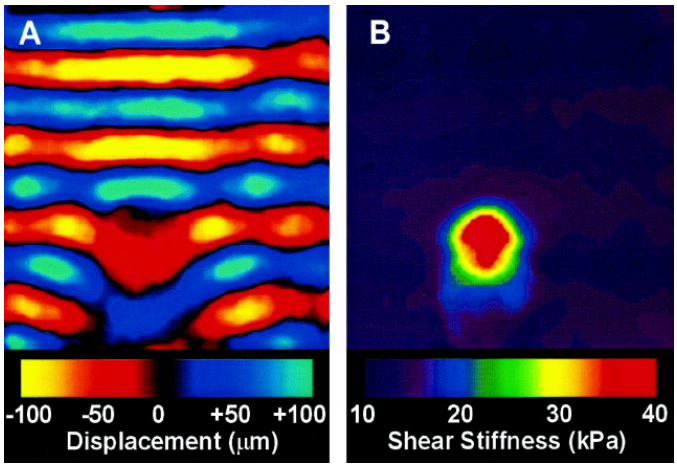

Figure 1.1: This figure is taken from Manduca et al. [14]. It shows MRE of a object with diameter comparable to the wavelength. (A) shows how the wave travels through the medium. In (B) the shear stiffness is depicted, it is clear where the object is located.

been obtained. The rheological properties of the liver are known from other studies, thus comparison is possible. The MR images were obtained at UW Madison on a 3T GE Scanner. The spatial resolution was 1.5625 mm $\times$ 1.5625 mm and 32 images were obtained. Software provided by the Mayo Clinic [11] have been used to create a wave map and an elastogram. This was done by Karen Støverud, before the data were given to me for further work. All simulations will be carried out using the Python interface of the finite element software FEniCS [12; 13]. All source code written for this thesis are available online at `bitbucket.org/istorpe/source-code-master-s-degree/` and an excerpt is also available in Appendix A.

The thesis has the following outline. Chapter 2 presents the mathematical models studied in this thesis. The finite element method is described in a short presentation in Chapter 3, together with derivation of finite element formulations of the chosen mathematical models. In Chapter 4 a study of Tikhonov regularization and synthetic noise in input data for the Poisson minimization problem is presented. In Chapter 5 a similar study is presented for the linear elasticity minimization problem. Results from experiments with real MRE data are presented in Chapter 6. Finally, a discussion of the findings and conclusions are given in Chapter 7.

Chapter 2

Mathematical models

This chapter presents two models describing deformation of a medium under external forces. The two models ate the Poisson equation and the linear elasticity equation. Both these models will be used in the later chapters.

2.1 The Poisson problem

Let Ω be an open and bounded domain in $\mathbb{R}^2$ with boundary $\partial\Omega$. The Poisson equation is given by

$$\nabla \cdot \mu \nabla u = f, \tag{2.1}$$

where $u = u(\boldsymbol{x})$, with $\boldsymbol{x} = (x_1, x_2)$, is the unknown function, $f = f(\boldsymbol{x})$ is a prescribed function and the parameter μ may be either a constant or a function varying through the domain. The operator $\nabla\cdot$ is the divergence operator and ∇ denotes the gradient.

In addition we consider pure Neumann boundary conditions:

$$\mu \frac{\partial u}{\partial \boldsymbol{n}} = \mu \nabla u \cdot \boldsymbol{n} = t, \tag{2.2}$$

on the whole boundary $\partial\Omega$, where t is some given function.

Doyley [15] reviews approaches of elastography and to the inverse elasticity problem. He divides the current approaches to MRE into three categories: quasi static elastography, harmonic elastography and transient elastography. In this thesis we study the deformation of biological tissue in harmonic elastography and to describe this deformation, we will assume the approximation $f \approx \rho\omega^2 u$. Using this assumption the arising equation is the steady-state equation describing harmonic deformation in an isotropic

medium [3; 15; 16]. Here, ρ denotes the density of the material and ω is the angular frequency of the sinusoidal wavefront transmitted within the tissue in the MRE examination.

Thus, the boundary value problem reads

$$\rho\omega^2 u - \nabla \cdot \mu \nabla u = 0 \quad \text{in } \Omega, \tag{2.3a}$$

$$\mu \frac{\partial u}{\partial \boldsymbol{n}} = t \quad \text{on } \partial\Omega. \tag{2.3b}$$

(2.3a) is also known as Helmholtz equation.

2.2 Linear elasticity

The linear elasticity equations describe the deformation of a purely elastic body, occupying a domain denoted $\Omega \subset \mathbb{R}^d$, with $d = 2, 3$, and boundary $\partial\Omega$. The following material is based on a book of Atkinson and Han [17]. Assume that an external body force $\boldsymbol{f}$ acts on the body and a traction force $\boldsymbol{t}$ acts on the surface and enforces deformation. The linearised elasticity equation arises from the equilibrium state the body reaches as a result of the act of the external body forces. As the body deforms, consider a point $\boldsymbol{x} \in \Omega$ in the body before applying the external forces. This point will be shifted to a new point $\boldsymbol{x} + \boldsymbol{u}$ after the deformation, due to the external forces. The displacement of the point $\boldsymbol{x}$ is thus given by a function $\boldsymbol{u} = \boldsymbol{u}(\boldsymbol{x})$ and $\boldsymbol{u} : \Omega \to \mathbb{R}^d$ is a vector-valued function. The equation of equilibrium the body reaches after the deformation takes the form

$$\nabla \cdot \boldsymbol{\sigma}(\boldsymbol{u}) = \boldsymbol{f} \quad \text{ in } \Omega \tag{2.4}$$

Here, $\boldsymbol{\sigma}$ is the stress tensor, which describes the internal forces per unit area neighbouring points of the body apply on each other. The stress tensor is a second order symmetric tensor on $\mathbb{R}^d$, and may be viewed as a symmetric matrix of size $d \times d$.

A stress-strain relation is a constitutive relation that describes the mechanical response of the material. In linear elasticity, this relation is expressed by Hooke's law

$$\boldsymbol{\sigma}(\boldsymbol{u}) = \boldsymbol{C}\boldsymbol{\varepsilon}(\boldsymbol{u}), \tag{2.5}$$

where $\boldsymbol{C}$ is the stiffness (or elasticity) tensor and $\boldsymbol{\varepsilon}$ is the infinitesimal strain tensor. When the deformation of the body is small, that is, both the displacement and the displacement gradient are small, the linearised strain tensor may be used. This tensor is defined as

$$\boldsymbol{\varepsilon}(\boldsymbol{u}) = \frac{1}{2}\Big(\nabla \boldsymbol{u} + (\nabla \boldsymbol{u})^T\Big). \tag{2.6}$$

The stiffness tensor is of fourth order, or in other words, it is a map between second order tensors. Depending on the material properties, this map may be independent on $\boldsymbol{x} \in \Omega$, then the material is homogeneous. Otherwise, if $\boldsymbol{C}$ is dependent on $\boldsymbol{x}$, the material is heterogeneous. Another important material property is isotropy. For some fixed point $\boldsymbol{x} \in \Omega$, the material is isotropic at $\boldsymbol{x}$ if $\boldsymbol{C}(\boldsymbol{x})$ is invariant with respect to rotations of the coordinate system, otherwise it is anisotropic at $\boldsymbol{x}$.

In the case of a homogeneous, isotropic linear elastic medium, the components of the elasticity tensor may be expressed as

$$C_{ijkl} = \mu(\delta_{ik}\delta_{jl} + \delta_{il}\delta_{jk}) + \lambda\delta_{ij}\delta_{kl}, \tag{2.7}$$

where λ, μ are the Lamé elasticity parameters and δ_{ij} is the Kronecker delta. Another common name for μ is the shear modulus. Using this expression for $\boldsymbol{C}$ leads to a new expression for the stress tensor:

$$\boldsymbol{\sigma}(\boldsymbol{u}) = 2\mu\boldsymbol{\varepsilon}(\boldsymbol{u}) + \lambda \operatorname{tr} \boldsymbol{\varepsilon}(\boldsymbol{u})\mathbf{I}. \tag{2.8}$$

Here, $\mathbf{I}$ denotes the second order unit tensor which may be thought of as the identity matrix. Thus, the linear elasticity equations becomes:

$$\nabla \cdot \boldsymbol{\sigma}(\boldsymbol{u}) = \boldsymbol{f} \qquad \text{in } \Omega, \tag{2.9a}$$

$$\boldsymbol{\sigma}(\boldsymbol{u}) = 2\mu\boldsymbol{\varepsilon}(\boldsymbol{u}) + \lambda \operatorname{tr}\Big(\boldsymbol{\varepsilon}(\boldsymbol{u})\Big)\mathbf{I} \quad \text{in } \Omega. \tag{2.9b}$$

Throughout this thesis (2.9b) will be used as the definition of the stress tensor.

Adding Neumann boundary conditions, we arrive at a linear elasticity boundary value problem. The Neumann conditions describes the action of the stress tensor, $\boldsymbol{\sigma}$, along the direction of the outward pointing normal vector, and take the form

$$\boldsymbol{\sigma}\boldsymbol{n} = \boldsymbol{t} \quad \text{on } \partial\Omega. \tag{2.10}$$

Here $\boldsymbol{n}$ is the outward pointing normal vector along the boundary and $\boldsymbol{t}$ is a given surface traction force.

The Lamé elasticity parameters in the stress tensor may be expressed in terms of material properties like Young's modulus, E, which is a measure of the stiffness of an elastic isotropic body, and Poisson's ratio, ν, which is the ratio of transverse contraction strain to longitudinal expansion strain [18]. These expressions are given as

$$\lambda = \frac{E\nu}{(1+\nu)(1-2\nu)}, \qquad \mu = \frac{E}{2(1+\nu)}. \tag{2.11}$$

The Lamé parameters are always positive, and if $\lambda >> \mu$, the material is nearly incompressible [18].

Similar as for the Poisson problem, described in Chapter 2.1, $\boldsymbol{f}$ is approximated by the displacement $\rho\omega^2\boldsymbol{u}$. The arising equation is the steady-state equation describing harmonic deformation in an isotropic, linear elastic medium [3; 15], which describes the action of an MRE examination. The elastic boundary value problem now reads:

$$\begin{aligned} \rho\omega^2\boldsymbol{u} - \nabla\cdot\boldsymbol{\sigma}(\boldsymbol{u}) &= \boldsymbol{0} \quad \text{in } \Omega, \\ \boldsymbol{\sigma}(\boldsymbol{u})\boldsymbol{n} &= \boldsymbol{t} \quad \text{on } \partial\Omega. \end{aligned} \tag{2.12}$$

2.3 PDE-constrained optimization

In this thesis we want to use a one-shot approach in PDE-constrained optimization to find the material parameters of tissue. In problems with PDE-constrained optimization (or minimization), one seeks to minimize a cost functional $J(u,\mu) \in \mathbb{R}$ subject to constraints [19; 20; 18]. A general PDE-constrained optimization problem takes the form:

$$\begin{aligned} &\min_{u,\mu} J(u,\mu) \\ \text{subject to } &F(u,\mu) = 0, \\ &h(u,\mu) = 0, \\ &g(u,\mu) \leq 0, \end{aligned} \tag{2.13}$$

where $F(u,\mu) = 0$ is a PDE or a system of PDEs with control or optimization parameter μ and solution u, and $h(u,\mu) = 0$ and $g(u,\mu) \leq 0$ are equality and inequality constraints, respectively, enforcing additional conditions to the minimization problem.

PDE-constrained optimization problems may be solved using various methods, in this thesis the one-shot method (also called the all-at-once method or the Lagrangian approach) will be used. This method is based on the theory on Lagrange multipliers and may be regarded as a search of extrema of the Lagrangian functional $\mathcal{L}$, which is defined as a sum of the cost functional and the weak constraint [20; 21]:

$$\mathcal{L}(u,\mu,w) = J(u,\mu) + \int_\Omega F(u,\mu)\, w \,\mathrm{d}x, \tag{2.14}$$

where w is the Lagrange multiplier (also called the dual or adjoint variable).

Regularization terms may also be added to constrain possible solutions further. Tikhonov regularization is the most commonly used method for regularization of ill-posed problems [15] and is the method that will be used

in this thesis. To describe the technique of Tikhonov regularization, we first need the definition of a well-posed problem. According to Evans [22] a problem is well-posed if

1. there exists a solution,
2. the solution is unique, and
3. the solution is continuously dependent of the data given in the problem.

A problem that is not well-posed is ill-posed. Vogel [23] defines regularization as it "*imposes stability on an ill-posed problem in a manner that yields accurate approximate solutions, often by incorporating prior information*". The technique of Tikhonov regularization is carried out as follows [24; 25]: If a problem $Ax = b$ is not well-posed, the standard technique to solve it is by least squares which seeks to minimize the residual $\|Ax - y\|^2$. In the case of Tikhonov regularization one adds an additional term $\alpha\|x\|^2$, to make this minimization problem well-posed. The parameter $\alpha > 0$ is the regularization parameter and the solution x that minimizes the problem $\|Ax - b\|^2 + \alpha\|x\|^2$ is called the regularized solution. In the regularization term one may also add prior knowledge, to minimize the difference between the unknown and the prior knowledge.

The solution of (u, μ) of the optimization problem (2.13) must satisfy the set of equations:

$$\begin{aligned} \frac{\partial \mathcal{L}}{\partial u} &= 0, \\ \frac{\partial \mathcal{L}}{\partial \mu} &= 0, \\ \frac{\partial \mathcal{L}}{\partial w} &= 0. \end{aligned} \tag{2.15}$$

2.3.1 The Poisson minimization problem

For the Poisson problem the minimization problem the cost functional to be minimized is

$$J(u, \mu) = \|u - u_{\text{MR}}\|^2_{L^2(\Omega)} + \alpha\|\mu - \mu_{\text{prior}}\|^2_{L^2(\Omega)}, \tag{2.16}$$

where we assume that u_{MR} is a known function from MR measurements. The second term, which minimizes the error in μ compared to μ_{prior} is a regularization term, where μ_{prior} serves as a target guess for μ. The solutions u, μ must satisfy the PDE

$$F(u, \mu) = \rho\omega^2 u - \nabla \cdot \mu \nabla u = 0$$

in Ω, and the boundary conditions

$$\mu \frac{\partial u}{\partial \boldsymbol{n}} = t$$

on the whole boundary $\partial\Omega$. Thus the optimization problem becomes: Find $u \in V$, $\mu \in S$, such that

$$\min_{u,\mu} \ \|u - u_{\mathrm{MR}}\|^2_{L^2(\Omega)} + \alpha \|\mu - \mu_{\mathrm{prior}}\|^2_{L^2(\Omega)} \tag{2.17a}$$

$$\text{subject to } \rho\omega^2 u - \nabla \cdot \mu \nabla u = 0, \tag{2.17b}$$

$$\mu \frac{\partial u}{\partial \boldsymbol{n}} = t, \tag{2.17c}$$

where V and S are some suitable function spaces to be defined in Chapter 3.

By the definition of the Lagrangian, the Lagrangian for the inverse Poisson problem becomes:

$$\begin{aligned} \mathcal{L}(u, \mu, w) =& J(u, \mu) + \int_\Omega F(u, \mu) w \, \mathrm{d}x \\ =& \int_\Omega (u - u_{\mathrm{MR}})^2 \, \mathrm{d}x + \int_\Omega (\rho\omega^2 u - \nabla \cdot \mu \nabla u) \, w \, \mathrm{d}x \\ &+ \alpha \int_\Omega (\mu - \mu_{\mathrm{prior}})^2 \, \mathrm{d}x, \end{aligned} \tag{2.18}$$

where w is the adjoint variable from a suitable function space Q to be defined in Chapter 3, α is the regularization parameter and μ_{prior} is a guess for the parameter μ. In the second term of the Lagrangian, second order derivatives appear. By integration by parts, these second order derivatives may be substituted by terms of only first order derivatives

$$\begin{aligned} \int_\Omega (\rho\omega^2 u - \nabla \cdot \mu \nabla u) \, w \, \mathrm{d}x &= \int_\Omega \rho\omega^2 u \, w \ \mathrm{d}x + \int_\Omega \mu \nabla u \cdot \nabla w \, \mathrm{d}x - \int_{\partial\Omega} \mu \nabla u \cdot \boldsymbol{n} \, w \, \mathrm{d}s \\ &= \int_\Omega \rho\omega^2 u \, w \, \mathrm{d}x + \int_\Omega \mu \nabla u \cdot \nabla w \, \mathrm{d}x - \int_{\partial\Omega} t w \, \mathrm{d}s. \end{aligned}$$

Inserting this into (2.18) yields

$$\begin{aligned} \mathcal{L}(u, \mu, w) = &\int_\Omega (u - u_{\mathrm{MR}})^2 \, \mathrm{d}x + \int_\Omega \rho\omega^2 u \, w \, \mathrm{d}x + \int_\Omega \mu \nabla u \cdot \nabla w \, \mathrm{d}x \\ &- \int_{\partial\Omega} t w \, \mathrm{d}s + \alpha \int_\Omega (\mu - \mu_{\mathrm{prior}})^2 \, \mathrm{d}x. \end{aligned} \tag{2.19}$$

2.3.2 Minimization of the linear elasticity problem

The minimization problem for the elasticity model is derived in the same manner as for the Poisson problem. Assume that $\boldsymbol{u}_{\mathrm{MR}}$ is known displacement from MR elastography and μ_{prior} and λ_{prior} are prior knowledge of μ

and λ. The cost functional is then defined as

$$J(u,\mu,\lambda) = \|u - u_{\mathrm{MR}}\|^2_{L^2(\Omega)} + \alpha\|\mu - \mu_{\mathrm{prior}}\|^2_{L^2(\Omega)} + \beta\|\lambda - \lambda_{\mathrm{prior}}\|^2_{L^2(\Omega)}. \tag{2.20}$$

Here both α and β are regularization parameters. The solutions u, μ and λ must satisfy the linear elasticity equations (2.9) and the boundary conditions (2.10). Thus the optimization problem reads: Find $u \in V$, $\mu, \lambda \in S$, such that

$$\min_{u,\mu} \ \|\boldsymbol{u} - \boldsymbol{u}_{\mathrm{MR}}\|^2_{L^2(\Omega)} + \alpha\|\mu - \mu_{\mathrm{prior}}\|^2_{L^2(\Omega)} + \beta\|\lambda - \lambda_{\mathrm{prior}}\|^2_{L^2(\Omega)} \tag{2.21a}$$

$$\text{subject to } \rho\omega^2\boldsymbol{u} - \nabla\cdot\boldsymbol{\sigma}(\boldsymbol{u}) = 0, \tag{2.21b}$$

$$\boldsymbol{\sigma}(\boldsymbol{u})\boldsymbol{n} = \boldsymbol{t}, \tag{2.21c}$$

The Lagrangian of the linear elasticity minimization problem becomes

$$\begin{aligned}\mathcal{L}(\boldsymbol{u},\mu,\lambda,\boldsymbol{w}) = &\int_\Omega (\boldsymbol{u} - \boldsymbol{u}_{\mathrm{MR}})^2 \,\mathrm{d}x + \int_\Omega (\rho\omega^2\boldsymbol{u} - \nabla\cdot\boldsymbol{\sigma}(\boldsymbol{u}))\cdot\boldsymbol{w}\,\mathrm{d}x \\ &+ \alpha\int_\Omega (\mu - \mu_{\mathrm{prior}})^2\,\mathrm{d}x + \beta\int_\Omega (\lambda - \lambda_{\mathrm{prior}})^2\,\mathrm{d}x.\end{aligned} \tag{2.22}$$

Integration by parts in the term with second order derivatives yield

$$\begin{aligned}\int_\Omega -\nabla\cdot\boldsymbol{\sigma}(\boldsymbol{u})\cdot\boldsymbol{w}\,\mathrm{d}x &= \int_\Omega \boldsymbol{\sigma}(\boldsymbol{u}) : \nabla\boldsymbol{w}\,\mathrm{d}x - \int_{\partial\Omega}\Big(\boldsymbol{\sigma}(\boldsymbol{u})\boldsymbol{n}\Big)\cdot\boldsymbol{u}\,\mathrm{d}s \\ &= \int_\Omega \boldsymbol{\sigma}(\boldsymbol{u}) : \nabla\boldsymbol{w}\,\mathrm{d}x - \int_{\partial\Omega}\boldsymbol{t}\cdot\boldsymbol{u}\,\mathrm{d}s,\end{aligned} \tag{2.23}$$

since $\boldsymbol{\sigma}(\boldsymbol{u})\boldsymbol{n} = \boldsymbol{t}$. Inserting this result into (2.22) gives

$$\begin{aligned}\mathcal{L}(\boldsymbol{u},\mu,\lambda,\boldsymbol{w}) = &\int_\Omega (\boldsymbol{u} - \boldsymbol{u}_{\mathrm{MR}})^2\,\mathrm{d}x + \int_\Omega \rho\omega^2\boldsymbol{u}\cdot\boldsymbol{w}\,\mathrm{d}x \\ &+ \int_\Omega \boldsymbol{\sigma}(\boldsymbol{u}) : \nabla\boldsymbol{w}\,\mathrm{d}x - \int_{\partial\Omega}\boldsymbol{t}\cdot\boldsymbol{w}\,\mathrm{d}s \\ &+ \alpha\int_\Omega (\mu - \mu_{\mathrm{prior}})^2\,\mathrm{d}x + \beta\int_\Omega (\lambda - \lambda_{\mathrm{prior}})^2\,\mathrm{d}x.\end{aligned} \tag{2.24}$$

Chapter 3

Numerical formulation

Since the 1960s, numerical methods has become an invaluable tool in solving PDEs. The use of computers in problem solving allows us to solve more complex problems and save a huge amount of time compared to solving them by hand. To solve the problems described in Chapter 2, the numerical method called the finite element method (FEM) will be used. This method is a popular and widely used method to solve PDEs [26].

3.1 The Finite element method: Linear PDEs

In this section a short description of the finite element method is given. This description of the finite element method is based on material of Kirby and Logg [27] and Brenner and Scott [28]. The finite element method are carried out as follows: Starting with the strong form of a PDE, derive a weak form, apply the Galerkin method on the weak form and finally solve a system of equations.

Beginning at the first step we consider a general strong form of a boundary value problem:

$$Lu = f \quad \text{in } \Omega \tag{3.1a}$$

$$u = u_0 \quad \text{on } \Gamma_{\mathrm{D}} \tag{3.1b}$$

$$\frac{\partial u}{\partial n} = g \quad \text{on } \Gamma_{\mathrm{N}} \tag{3.1c}$$

where L is a linear differential operator, u is the unknown function and f is some given source term. The boundaries Γ_{D} and Γ_{N} are Dirichlet and Neumann boundaries, respectively, and $\Gamma_{\mathrm{D}} \cup \Gamma_{\mathrm{N}} = \partial\Omega$ and $\Gamma_{\mathrm{D}} \cap \Gamma_{\mathrm{N}} = \emptyset$.

In the weak form (also called variational form) one searches for a solution u in a trial space V. To derive the weak form of (3.1a), multiply the strong form by some test function, $v \in \hat{V}$, and integrate over the domain Ω:

$$\int_\Omega (Lu)v \,\mathrm{d}x = \int_\Omega fv \,\mathrm{d}x \tag{3.2}$$

In the left hand side term there might be derivatives of higher order. These terms may be reduced to be of only first order by performing integration by parts. The space $\hat{V}$ is called a test space and the spaces V and $\hat{V}$ should be defined so that the boundary conditions defined in (3.1b) are satisfied. The weak form becomes: Find $u \in V$ such that

$$a(u, v) = l(v) \tag{3.3}$$

for all $v \in \hat{V}$, where $a : V \times \hat{V} \to \mathbb{R}$, defined by $a(u, v) = \int_\Omega (Lu)v \,\mathrm{d}x$, is called the bilinear form and $l : \hat{V} \to \mathbb{R}$, defined by $l(v) = \int_\Omega fv \,\mathrm{d}x$, is called the linear form.

To solve the variational problem and find the finite element solution, the next step is to define finite-dimensional trial and test spaces. Let $V_h \subset V$ be finite-dimensional and let $\{\varphi_j\}_{j=1}^N$ be a basis for V_h. Also let $\hat{V}_h \subset \hat{V}$ be finite-dimensional and assume $\{\hat{\varphi}_i\}_{i=1}^N$ to be a basis for $\hat{V}_h$. N is the dimension of both V_h and $\hat{V}_h$. Assume the approximation $u_h \approx u$, where $u_h \in V_h$, thus u_h has N degrees of freedom. Replacing u by the approximation u_h in (3.3) leads to the discrete variational problem: Find $u_h \in V_h$ such that

$$a(u_h, v) = l(v) \tag{3.4}$$

for all $v \in \hat{V}_h \subset \hat{V}$.

We make an ansatz for u_h in terms of the trial space's basis functions

$$u_h(x) = \sum_{j=1}^{N} U_j \varphi_j(x), \tag{3.5}$$

where U_j are coefficients which defines the degrees of freedom of u_h. Inserting (3.5) into (3.4) and letting the test function $v = \hat{\varphi}_i$, leads to a linear system of equations:

$$a\left(\sum_{j=1}^{N} U_j \varphi_j, \hat{\varphi}_i\right) = l(\hat{\varphi}_i), \quad i = 1, \ldots, N, \tag{3.6}$$

which may be rewritten as

$$\sum_{j=1}^{N} U_j a(\varphi_j, \hat{\varphi}_i) = l(\hat{\varphi}_i), \quad i = 1, \ldots, N. \tag{3.7}$$

This is a linear algebraic system of equations, and may be represented in matrix form as

$$AU = b, \tag{3.8}$$

where

$$\begin{aligned} A_{ij} &= a(\varphi_j, \varphi_i), \quad \text{for } i,j = 1,\dots,N \\ b_i &= l(\varphi_i), \qquad \text{for } i = 1,\dots,N \end{aligned} \tag{3.9}$$

and $\{U_j\}_{j=1}^N \in \mathbb{R}^N$ is the vector of degrees of freedom of u_h.

For the error in the approximation u_h compared to the exact solution u, we will in later chapters consider the L^2-norm and the H^1-norm. These norms are defined as

$$E_0 = \|u_h - u\|_{L^2(\Omega)} = \left(\int_\Omega (u_h - u)^2 \, \mathrm{d}x \right)^{1/2}, \tag{3.10}$$

$$\begin{aligned} E_1 &= \|u_h - u\|_{H^1(\Omega)} \\ &= \left(\int_\Omega (u_h - u)^2 \, \mathrm{d}x + \int_\Omega \left(\nabla(u_h - u) \right)^2 \mathrm{d}x \right)^{1/2}, \end{aligned} \tag{3.11}$$

respectively.

3.2 The finite element method: Nonlinear PDEs

Nonlinear problems may also be solved elegantly using FEM. Consider the general variational form: Find $u \in V$ such that

$$F(u; v) = 0 \tag{3.12}$$

for all $v \in \hat{V}$, where $F : V \times \hat{V} \to \mathbb{R}$ is a semilinear form. A semilinear form may be nonlinear in the argument appearing in front of the semicolon and is linear in the argument which appears after the semicolon.

Again, let V_h be a finite dimensional subspace of V and $\hat{V}_h$ a finite dimensional subspace of $\hat{V}$. The corresponding discrete variational problem reads: Find $u_h \in V_h$ such that

$$F(u_h; v) = 0 \tag{3.13}$$

for all $v \in \hat{V}_h$. By expressing u_h in terms of the given basis, a system of equations are obtained

$$F\left(\sum_{j=1}^N U_j \varphi_j; \hat{\varphi}_i \right) = 0. \tag{3.14}$$

This is a nonlinear system of equations. Such systems are solved effectively using iterative methods. In this thesis, Newton's iterative method [29] will be used.

3.3 Newton's method

The starting point of Newton's method is a nonlinear system of equations, such as (3.13). In the following we have $x = u_h$ and $G(\cdot) = F(\cdot; v)$. The Taylor series expansion of G around y is

$$G(x) = G(y) + J(y)(x - y) + \mathcal{O}\Big((x - y)^2\Big), \tag{3.15}$$

where J is the Jacobian of G defined by

$$J_{ij}(x) = \frac{\partial F_i(x)}{\partial x_j}. \tag{3.16}$$

We introduce the linear approximation $\hat{G}$ of G:

$$\hat{G}(x) = G(y) + J(y)(x - y). \tag{3.17}$$

Denote $\delta x = x - y$. Newton's method is based on iteratively solving

$$\hat{G}(x) = 0 \tag{3.18}$$

and updating the value of x [26]:

$$x = y + \delta x. \tag{3.19}$$

Letting the unknown x be indexed with an iteration counter, and letting the known y be the solution of the previous iteration, the algorithm for Newton's method becomes as follows: Given $G(x) = 0$ and an initial guess $x^0 = y$, repeat the iteration steps

1. Solve $J(x^k)(\delta x)^{k+1} = -G(x^k)$, and
2. update $x^{k+1} = x^k + (\delta x)^{k+1}$.

Iterations continue until the the following convergence criteria are met:

$$\|G(x^{k+1})\| \leq \epsilon_{\text{abs}}, \tag{3.20a}$$

$$\frac{\|G(x^{k+1})\|}{g(x^0)} \leq \epsilon_{\text{rel}}, \tag{3.20b}$$

where ϵ_{abs} is the absolute convergence criterion and ϵ_{abs} is the relative convergence criterion.

In Newton's method it is sometimes desirable to make smaller changes in each iteration. This can be done by multiplying the second term in the update of x^{x+1} by a constant $0 < \omega_{\text{rel}} < 1$, in the standard Newton's method, this parameter equals 1.0. Thus the iteration algorithm for the relaxed Newton's method becomes [26]

1. Solve $J(x^k)(\delta x)^{k+1} = -G(x^k)$, and
2. update $x^{k+1} = x^k + \omega_{\text{rel}}(\delta x)^{k+1}$.

If the relaxation parameter is < 1, it is called under-relaxation and makes the change done in each iteration smaller.

3.4 Finite element formulation of the inverse Poisson problem

The finite element method will be used to solve the Poisson minimization problem numerically. Following the description given in Chapter 3.2, we begin with Lagrangian of the problem, given in (2.19) and reads:

$$\begin{aligned}\mathcal{L}(u,\mu,w) = &\int_\Omega (u-u_{\text{MR}})^2 \,\mathrm{d}x + \int_\Omega \rho\omega^2 u\, w \,\mathrm{d}x + \int_\Omega \mu\nabla u\cdot\nabla w \,\mathrm{d}x \\ &- \int_{\partial\Omega} tw \,\mathrm{d}s + \alpha\int_\Omega (\mu-\mu_{\text{prior}})^2 \,\mathrm{d}x.\end{aligned}$$

The variational form of the minimization problem is derived by taking the derivatives of the Lagrangian in the directions of the test functions: Find $(u,\mu,w) \in V\times S\times Q$ such that

$$\frac{\partial\mathcal{L}}{\partial u}[v] = \frac{\partial\mathcal{L}}{\partial\mu}[\eta] = \frac{\partial\mathcal{L}}{\partial w}[q] = 0. \tag{3.21}$$

for all $(v,\eta,q) \in \hat{V}\times\hat{S}\times\hat{Q}$. Here we let $V = \hat{V} = H^1(\Omega)$, $S = \hat{S} = L^2(\Omega)$ and $Q = \hat{Q}s = H^1(\Omega)$, where $H^1(\Omega)$ is the Sobolev space of square Lebesgue integrable functions with square integrable derivatives and $L^2(\Omega)$ is the Sobolev space of square Lebesgue integrable functions.

(3.21) solves the minimization problem in (2.15), since

$$\frac{\partial\mathcal{L}}{\partial u} = 0 \quad\Longleftrightarrow\quad \frac{\partial\mathcal{L}}{\partial u}[v] = 0 \quad \forall\, v\in\hat{V}, \tag{3.22}$$

and equivalently for the other derivatives [25]. To compute the directional derivative, we define the Gâteaux derivative [25]:

$$\frac{\partial\mathcal{L}}{\partial u}[v] = \lim_{\epsilon\to 0}\frac{\mathcal{L}(u+\epsilon v,\mu,w)-\mathcal{L}(u,\mu,w)}{\epsilon} = \frac{d}{d\epsilon}\Big[\mathcal{L}(u+\epsilon v,\mu,w)\Big]_{\epsilon=0} \tag{3.23}$$

Thus, the directional derivative of the Lagrangian along v is:

$$\begin{aligned}\frac{\partial \mathcal{L}}{\partial u}[v] &= \frac{d}{d\epsilon}\Big[\int_\Omega (u+\epsilon v - u_{\mathrm{MR}})^2 \,\mathrm{d}x + \int_\Omega \rho\omega^2 (u+\epsilon v) w \,\mathrm{d}x \\ &\qquad + \int_\Omega \mu \nabla(u+\epsilon v)\cdot\nabla w \,\mathrm{d}x - \int_{\partial\Omega} t w \,\mathrm{d}s \\ &\qquad + \alpha \int_\Omega (\mu - \mu_{\mathrm{prior}})^2 \,\mathrm{d}x\Big]_{\epsilon=0} \\ &= \Big[\int_\Omega 2(u+\epsilon v - u_{\mathrm{MR}})\, v \,\mathrm{d}x + \int_\Omega \rho\omega^2 v\, w \,\mathrm{d}x + \int_\Omega \mu \nabla v\cdot\nabla w \,\mathrm{d}x\Big]_{\epsilon=0} \\ &= 2\int_\Omega (u - u_{\mathrm{MR}})\, v \,\mathrm{d}x + \int_\Omega \rho\omega^2 v\, w \,\mathrm{d}x + \int_\Omega \mu \nabla v\cdot\nabla w \,\mathrm{d}x\end{aligned}$$

for all $v \in \hat{V}$. The other directional derivatives are computed in the same manner and become:

$$\frac{\partial \mathcal{L}}{\partial \mu}[\eta] = \int_\Omega \eta \nabla u\cdot\nabla w \,\mathrm{d}x + 2\alpha \int_\Omega (\mu - \mu_{\mathrm{prior}})\eta \,\mathrm{d}x$$

for all $\eta \in \hat{S}$, and

$$\frac{\partial \mathcal{L}}{\partial w}[q] = \int_\Omega \rho\omega^2 u\, q \,\mathrm{d}x + \int_\Omega \mu \nabla u\cdot\nabla q \,\mathrm{d}x - \int_{\partial\Omega} t\, q \,\mathrm{d}s$$

for all $\eta \in \hat{Q}$.

Using the syntax from Chapter 3.2, the variational form of the Poisson minimization problem reads: Find $(u, \mu, w) \in V \times S \times Q$, such that

$$F((u,\mu,w);(v,\eta,q)) = 0 \tag{3.24}$$

for all $(v, \eta, q) \in \hat{V} \times \hat{S} \times \hat{Q}$, where

$$F((u,\mu,w);(v,\eta,q)) = \frac{\partial \mathcal{L}}{\partial u}[v] + \frac{\partial \mathcal{L}}{\partial \mu}[\eta] + \frac{\partial \mathcal{L}}{\partial w}[q]. \tag{3.25}$$

Let $V_h \subset V$, $S_h \subset S$ and $Q_h \subset Q$ be finite dimensional spaces and let $u_h \in V_h, \mu_h \in S_h$ and $w_h \in Q_h$ The discrete form is found by replacing u, μ, w by the discrete counterparts u_h, μ_h, w_h. In this thesis we let $V_h = \hat{V}_h$ be the space of continuous piecewise linear polynomials, let $S_h = \hat{S}_h$ be the space of piecewise constant functions and let $Q_h = \hat{Q}_h = V_h$. The discrete variational form reads: Find $(u_h, \mu_h, w_h) \in V_h \times S_h \times Q_h$, such that

$$F((u_h,\mu_h,w_h),(v,\eta,q)) = 0 \tag{3.26}$$

for all $(v, \eta, q) \in \hat{V}_h \times \hat{S}_h \times \hat{Q}_h$, where

$$F((u_h,\mu_h,w_h),(v,\eta,q)) = \frac{\partial \mathcal{L}}{\partial u_h}[v] + \frac{\partial \mathcal{L}}{\partial \mu_h}[\eta] + \frac{\partial \mathcal{L}}{\partial w_h}. \tag{3.27}$$

This problem may now be solved using Newton's method.

3.5 Finite element formulation of the inverse linear elasticity problem

To solve the linear elasticity minimization problem numerically we follow the same procedure as for the Poisson minimization problem and start with the Lagrangian given in (2.24):

$$\begin{aligned}\mathcal{L}(\boldsymbol{u},\mu,\lambda,\boldsymbol{w}) = &\int_\Omega (\boldsymbol{u}-\boldsymbol{u}_{\mathrm{MR}})^2\,\mathrm{d}x + \int_\Omega \rho\omega^2\boldsymbol{u}\cdot\boldsymbol{w}\,\mathrm{d}x \\ &+ \int_\Omega \boldsymbol{\sigma}(\boldsymbol{u}) : \nabla\boldsymbol{w}\,\mathrm{d}x - \int_{\partial\Omega}\boldsymbol{t}\cdot\boldsymbol{w}\,\mathrm{d}s \\ &+ \alpha\int_\Omega(\mu-\mu_{\mathrm{prior}})^2\,\mathrm{d}x + \beta\int_\Omega(\lambda-\lambda_{\mathrm{prior}})^2\,\mathrm{d}x.\end{aligned}$$

The variational formulation of the elasticity minimization problem is given by taking the directional derivatives of the Lagrangian along the directions of the test functions: Find $(\boldsymbol{u},\mu,\lambda,\boldsymbol{w})$ in $V\times S\times S\times Q$ such that

$$\frac{\partial\mathcal{L}}{\partial\mu}[\boldsymbol{v}] = \frac{\partial\mathcal{L}}{\partial\mu}[\eta] = \frac{\partial\mathcal{L}}{\partial\lambda}[\kappa] = \frac{\partial\mathcal{L}}{\partial\boldsymbol{w}}[\boldsymbol{q}] = 0 \tag{3.28}$$

for all $(\boldsymbol{v},\eta,\kappa,\boldsymbol{q})$ in $\hat{V}\times\hat{S}\times\hat{S}\times\hat{Q}$. We use the same function spaces for the Poisson problem for the parameters μ and λ, that is $S = L^2(\Omega)$, and we let $V = Q = [H^1(\Omega)]^d$. Let the test spaces equal the trial spaces.

By the definition of the Gâteaux derivative, the directional derivative of the

Lagrangian in $\boldsymbol{u}$ along $\boldsymbol{v}$ is:

$$\begin{aligned}
\frac{\partial \mathcal{L}}{\partial \boldsymbol{u}}[\boldsymbol{v}] &= \frac{d}{d\epsilon}\Big[\mathcal{L}(\boldsymbol{u}+\epsilon\boldsymbol{v},\mu,\lambda,\boldsymbol{w})\Big]_{\epsilon=0} \\
&= \frac{d}{d\epsilon}\Big[\int_\Omega (\boldsymbol{u}+\epsilon\boldsymbol{v}-\boldsymbol{u}_{\mathrm{MR}})^2\,\mathrm{d}x + \int_\Omega \rho\omega^2(\boldsymbol{u}+\epsilon\boldsymbol{v})\cdot\boldsymbol{w}\,\mathrm{d}x \\
&\qquad + \int_\Omega 2\mu\boldsymbol{\varepsilon}(\boldsymbol{u}+\epsilon\boldsymbol{v}) : \nabla\boldsymbol{w}\,\mathrm{d}x \\
&\qquad + \int_\Omega \lambda\,\mathrm{tr}\Big(\boldsymbol{\varepsilon}(\boldsymbol{u}+\epsilon\boldsymbol{v})\Big)\,\mathrm{tr}(\nabla\boldsymbol{w})\,\mathrm{d}x \\
&\qquad - \int_{\partial\Omega} \boldsymbol{t}\cdot\boldsymbol{w}\,\mathrm{d}s + \alpha\int_\Omega(\mu-\mu_{\mathrm{prior}})^2\,\mathrm{d}x \\
&\qquad + \beta\int_\Omega(\lambda-\lambda_{\mathrm{prior}})^2\,\mathrm{d}x\Big]_{\epsilon=0} \\
&= \Big[\int_\Omega 2(\boldsymbol{u}+\epsilon\boldsymbol{v}-\boldsymbol{u}_{\mathrm{MR}})\cdot\boldsymbol{v}\,\mathrm{d}x + \int_\Omega \rho\omega^2\boldsymbol{v}\cdot\boldsymbol{w}\,\mathrm{d}x \\
&\qquad + \int_\Omega 2\mu\boldsymbol{\varepsilon}(\boldsymbol{v}) : \nabla\boldsymbol{w}\,\mathrm{d}x + \int_\Omega \lambda\,\mathrm{tr}\Big(\boldsymbol{\varepsilon}(\boldsymbol{v})\Big)\,\mathrm{tr}(\nabla\boldsymbol{w})\,\mathrm{d}x\Big]_{\epsilon=0} \\
&= 2\int_\Omega(\boldsymbol{u}-\boldsymbol{u}_{\mathrm{MR}})\cdot\boldsymbol{v}\,\mathrm{d}x + \int_\Omega\rho\omega^2\boldsymbol{v}\cdot\boldsymbol{w}\,\mathrm{d}x \\
&\qquad + \int_\Omega 2\mu\boldsymbol{\varepsilon}(\boldsymbol{v}) : \nabla\boldsymbol{w}\,\mathrm{d}x + \int_\Omega \lambda\,\mathrm{tr}\Big(\boldsymbol{\varepsilon}(\boldsymbol{v})\Big)\,\mathrm{tr}(\nabla\boldsymbol{w})\,\mathrm{d}x.
\end{aligned}$$

By similar computations, the remaining three derivatives become

$$\begin{aligned}
\frac{\partial \mathcal{L}}{\partial \mu}[\eta] &= \int_\Omega 2\eta\boldsymbol{\varepsilon}(\boldsymbol{u}) : \nabla\boldsymbol{w}\,\mathrm{d}x + 2\alpha\int_\Omega(\mu-\mu_{\mathrm{MR}})\eta\,\mathrm{d}x, \\
\frac{\partial \mathcal{L}}{\partial \lambda}[\kappa] &= \int_\Omega \kappa\,\mathrm{tr}\Big(\boldsymbol{\varepsilon}(\boldsymbol{u})\Big)\,\mathrm{tr}(\nabla\boldsymbol{w})\,\mathrm{d}x + 2\beta\int_\Omega(\lambda-\lambda_{\mathrm{MR}})\kappa\,\mathrm{d}x, \\
\frac{\partial \mathcal{L}}{\partial \boldsymbol{w}}[\boldsymbol{q}] &= \int_\Omega \rho\omega^2\boldsymbol{u}\cdot\boldsymbol{q}\,\mathrm{d}x + \int_\Omega 2\mu\boldsymbol{\varepsilon}(\boldsymbol{u}) : \nabla\boldsymbol{q}\,\mathrm{d}x \\
&\qquad + \int_\Omega \lambda\,\mathrm{tr}\Big(\boldsymbol{\varepsilon}(\boldsymbol{u})\Big)\,\mathrm{tr}(\nabla\boldsymbol{q})\,\mathrm{d}x. - \int_{\partial\Omega}\boldsymbol{t}\cdot\boldsymbol{q}\,\mathrm{d}s.
\end{aligned}$$

Still, let $V_h \subset V$, $S_h \subset S$ and $Q_h \subset Q$ and similar for the test spaces. Let V_h and Q_h be the d-dimensional space of continuous piecewise linear polynomials and let S_h be the space of piecewise constant functions. Inserting the discrete approximations $u_h, \mu_h, \lambda_h, w_h$ of u, μ, λ, w into the variational form, the discrete variational form reads: Find $(\boldsymbol{u}_h, \mu_h, \lambda_h, \boldsymbol{w}_h)$ in $V_h \times S_h \times S_h \times Q_h$ such that

$$F((\boldsymbol{u}_h, \mu_h, \lambda_h, \boldsymbol{w}_h); (\boldsymbol{v}, \eta, \kappa, \boldsymbol{q})) = 0 \tag{3.29}$$

for all $(\boldsymbol{v}, \eta, \kappa, \boldsymbol{q})$ in $\hat{V}_h \times \hat{S}_h \times \hat{S}_h \times \hat{Q}_h$, where

$$F((\boldsymbol{u}_h, \mu_h, \lambda_h, \boldsymbol{w}_h); (\boldsymbol{v}, \eta, \kappa, \boldsymbol{q})) = \frac{\partial \mathcal{L}}{\partial \boldsymbol{u}_h}[\boldsymbol{v}] + \frac{\partial \mathcal{L}}{\partial \mu_h}[\eta] + \frac{\partial \mathcal{L}}{\partial \lambda_h}[\kappa] + \frac{\partial \mathcal{L}}{\partial \boldsymbol{w}_h}[\boldsymbol{q}]. \tag{3.30}$$

As for the Poisson problem, this problem may now be solved using Newton's method.

Chapter 4

Study of Tikhonov regularization for the Poisson equation

The numerical work in this thesis has been carried out using the FEM software FEniCS [13; 12]. For both the Poisson problem and the linear elasticity problem, solvers have been implemented in Python and experiments have been carried out to verify solvers. The source code used in this chapter can be found in Appendix A and is also available online at `bitbucket.org/istorpe/source-code-master-s-degree`. Sufficient knowledge of FEniCS to understand the code may be obtained by reading the FEniCS tutorial [30] and for more information about weak formulation of PDEs in FEniCS reading about UFL[21].

Consider the minimization problem given in (3.26) and (3.27)

$$F((u_h, \mu_h, w_h), (v, \eta, q)) = 0$$

for all $(v, \eta, q) \in \hat{V}_h \times \hat{S}_h \times \hat{Q}_h$, where

$$F((u_h, \mu_h, w_h), (v, \eta, q)) = \frac{\partial \mathcal{L}}{\partial u_h}[v] + \frac{\partial \mathcal{L}}{\partial \mu_h}[\eta] + \frac{\partial \mathcal{L}}{\partial w_h}.$$

Through this chapter we will study how Tikhonov regularization and noise in the input data affects the solutions of this optimization problem. Moreover, we will derive an analytical manufactured solution, the numerical solutions can be compared to the exact solutions and convergence rates can be computed based on the errors.

4.1 A manufactured solution of the Poisson minimization problem

Let the spatial domain be $\Omega = [0,1] \times [0,1]$, the unit square, and let the solution be given as

$$u(x,y) = e^{-kx} \tag{4.1}$$

for some integer k. Inserting this solution to the strong form (2.17b), μ may be calculated by direct inversion. The gradient and Laplacian of u are

$$\nabla u(x,y) = (\partial_x u, \partial_y u) = (-ke^{-kx}, 0) \tag{4.2}$$

$$\Delta u(x,y) = \partial_x(-ke^{-kx}) + \partial_y(0) = k^2 e^{-kx} = k^2 u(x,y). \tag{4.3}$$

Inserting these results to Eq. (2.3a) and assuming μ is constant, leads to

$$\rho\omega^2 u - \mu k^2 u = 0.$$

For simplicity, let $\rho\omega^2 = 1$, then solving for μ gives the analytical solution

$$\mu = \frac{1}{k^2}. \tag{4.4}$$

It is important to check that the boundary conditions are fulfilled to ensure a well-posed problem. The boundary conditions (2.17c) are pure Neumann conditions, that is, the value of the normal derivative of u is prescribed on all four sides of the unit square. First, consider the left boundary of the domain, where $x = 0$. Then the outward pointing normal vector is given by $\boldsymbol{n}_{left} = (-1, 0)$, this leads to the boundary condition

$$\begin{aligned} t_{left} &= \left(\frac{1}{k^2}\nabla u \cdot \boldsymbol{n}_{left}\right)\Big|_{x=0} = \left(-\frac{1}{k}e^{-kx}, 0\right) \cdot (-1,0)\Big|_{x=0} \\ &= \frac{1}{k}e^{-kx}\Big|_{x=0} = \frac{1}{k}. \end{aligned}$$

Next; on the right hand side boundary, where $x = 1$, the outward pointing normal vector is $\boldsymbol{n}_{right} = (1, 0)$, and the boundary conditions must be

$$t_{right} = \left(-\frac{1}{k}e^{-kx}, 0\right) \cdot (1,0)\Big|_{x=1} = -\frac{1}{k}e^{-kx}\Big|_{x=1} = -\frac{1}{k}e^{k}.$$

Finally, similar computations carried out for the top and bottom of the unit square yields

$$\begin{aligned} t_{top} &= \left(-\frac{1}{k}e^{-kx}, 0\right) \cdot (0,-1)\Big|_{y=0} = 0 \\ t_{bottom} &= \left(-\frac{1}{k}e^{-kx}, 0\right) \cdot (0,1)\Big|_{y=1} = 0. \end{aligned}$$

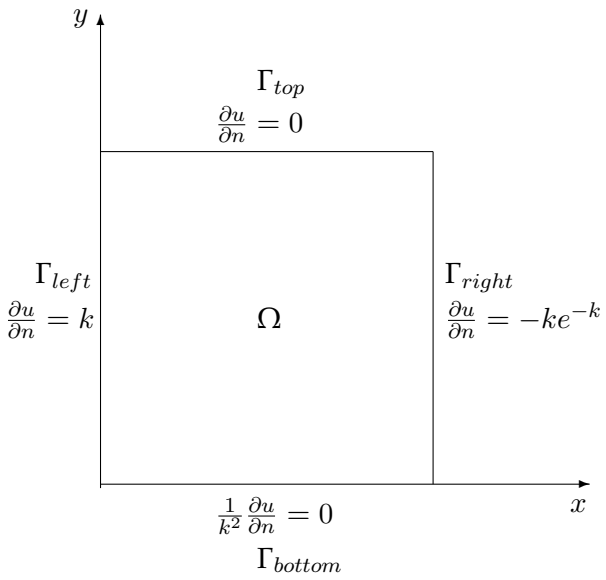

Figure 4.1: Sketch of the Poisson problem with $\mu = \frac{1}{k^2}$ throughout the domain Ω and Neumann conditions on the boundaries.

Thus, the boundary value problem is given by

$$\begin{aligned} u - \nabla \cdot \frac{1}{k^2}\nabla u &= 0 \qquad \text{in } \Omega \\ \frac{\partial u}{\partial n} &= k \qquad \text{on } \Gamma_{left} \\ \frac{\partial u}{\partial n} &= ke^{-k} \quad \text{on } \Gamma_{right} \\ \frac{\partial u}{\partial n} &= 0 \qquad \text{on } \Gamma_{top} \cup \Gamma_{bottom}, \end{aligned} \tag{4.5}$$

where Γ_{left}, Γ_{right}, Γ_{top}, and Γ_{bottom} denote the left, right, top and bottom sides of the unit square, respectively, and $\Gamma_{left} \cup \Gamma_{right} \cup \Gamma_{top} \cup \Gamma_{bottom} = \partial\Omega$.

To solve the minimization problem outlined in Chapter 2.3, expressions for u_{MR} and μ_{prior} are needed. The target solution of u, u_{MR}, is the displacement measured in the MRE measurements. Thus, in these experiments with constructed data u_{exact} is the target solution. however, in real MR elastography data, there will be noise in the measurement data, thus some white Gaussian noise will also be added to the exact solution to study how the noise affects the solutions. The amount of noise in the measured data is uncertain, thus adding various amounts of synthetic noise, will give an indication on how this affect the solution. Let u_{MR} be calculated in the

following way:

$$u_{\text{MR}} = u_{\text{exact}} + \mathcal{N}(0, \Delta_{\text{noise}}) \|u_{\text{exact}}\|_{L^2(\Omega)}. \tag{4.6}$$

Here, $\mathcal{N}(0, \Delta_{\text{noise}})$ is a Gaussian distribution with mean 0 and standard deviation (SD) Δ_{noise}. Δ_{noise} is the maximum percentage of noise added. In a study of the one-shot optimization with applications to ultrasound and MR by Oberai et al. [10], the amounts of noise considered are 3%, 1% and 0.3%. In the following experiments we consider $\Delta_{\text{noise}} = 0.1, 0.03, 0.01, 0.003, 0.0$.

As target solutions for μ, that is μ_{prior}, we consider both

$$\mu_{\text{prior}}(x, y) = \frac{1}{k^2}, \tag{4.7}$$

which is the exact solution from the manufactured problem, and

$$\mu_{\text{prior}}(x, y) = 0. \tag{4.8}$$

In the experiments we use $k = 2$, thus the analytical solutions are:

$$\begin{aligned} u_{\text{exact}} &= e^{-2x} \\ \mu_{\text{exact}} &= \frac{1}{2^2} = \frac{1}{4} \end{aligned} \tag{4.9}$$

4.2 Experiments and results with the Poisson minimization problem

Consider the following scenarios:

- μ in $\mathbb{R}$ vs. DG_0
- Varying regularization parameter, α
- $\mu_{\text{prior}} = 0$ vs. $\mu_{\text{prior}} = \mu_{\text{exact}}$
- Adding white Gaussian noise to u_{MR}

Materials may be either homogeneous or heterogeneous, thus we will test searching for both a constant parameter μ, that is $\mu \in \mathbb{R}$, and a parameter μ varying through the domain, that is $\mu \in \text{DG}_0$. DG is the discontinuous Galerkin space and DG_0 the discontinuous Galerkin space of degree 0, that is the space of piecewise constants. When using the one-shot approach for solving the inverse problem it might be useful to test with varying values for the regularization parameter α, and how this affect the result. In the regularization term the variable μ_{prior} prior appears as a target, or a guess, for the solution of μ and it is therefore interesting to observe how the value of this variable influence the solution of μ.

For the error in u consider both the in L^2-norm and the H^1-norm, and for the error in μ consider the L^2-norm:

$$\begin{aligned} E_{0,u} &= \|u_{\text{exact}} - u\|_{L^2(\Omega)}, \\ E_{1,u} &= \|u_{\text{exact}} - u\|_{H^1(\Omega)}, \\ E_{\mu} &= \|\mu_{\text{exact}} - \mu\|_{L^2(\Omega)}. \end{aligned} \tag{4.10}$$

The convergence rates are computed in the following way:

$$r_i = \frac{\log(E_i/E_{i-1})}{\log(h_i/h_{i-1})}, \tag{4.11}$$

where index i indicate the mesh size, E is the error and $h = 1/N$ is the discretization parameter. Sometimes this definition of h may give artefacts, but as we only study meshes with equal element sizes, this definition is satisfactory here. The mesh sizes considered are $N \times N$ for $N = 8, 16, 32, 64, 128$.

The experiments are carried out using the following initial guesses for the unknowns in the Newton solver:

$$\begin{aligned} u_0 &= u_{\text{exact}} \\ \mu_0 &= \mu_{\text{exact}} \\ w_0 &= 1.0 \end{aligned} \tag{4.12}$$

The parameters in the Newton solver are also as the previous experiments: 40 iterations are the maximum number of iterations, the absolute tolerance is 10^{-13} and the relative tolerance is set to 10^{-12}.

In the following section the results from the experiments are presented.

4.2.1 Minimization with homogeneous material without prior knowledge

We start by studying the simplest case, i.e. without regularization and without noise in the target solution of u. Table 4.1 shows the convergence rates in this case and we observe that the convergence rates of the error of u in L^2-norm converge to 2, the convergence rates of the error of u in H^1-norm converge to 1 and the convergence rates of the error of μ in L^2-norm converge to 2. This convergence rates are the optimal rates. The solutions are shown in Figure 4.2.

The next case to be considered is adding noise to the data. Can we still obtain high quality solutions? Let $\alpha = 10^{-5}$ and let varying noise be added to u_{MR}. The errors of the solutions are presented in Figure 4.3. For the error of u in L^2-norm, we observe that the error decreases as the discretization

N	$E_{0,u}$	rates	$E_{1,u}$	rates	E_{μ}	rates
8	1.888E-03		7.083E-02		4.794E-04	
16	4.779E-04	1.982	3.565E-02	0.991	1.190E-04	2.010
32	1.199E-04	1.995	1.786E-02	0.997	2.954E-05	2.011
64	3.001E-05	1.998	8.936E-03	0.999	7.358E-06	2.005
128	7.505E-06	2.000	4.469E-03	1.000	1.837E-06	2.002

Table 4.1: Convergence rates with $\alpha = 0.0$ and $\Delta_{\text{noise}} = 0.0$ when $\mu \in \mathbb{R}$ and $\mu_{\text{prior}} = 0$.

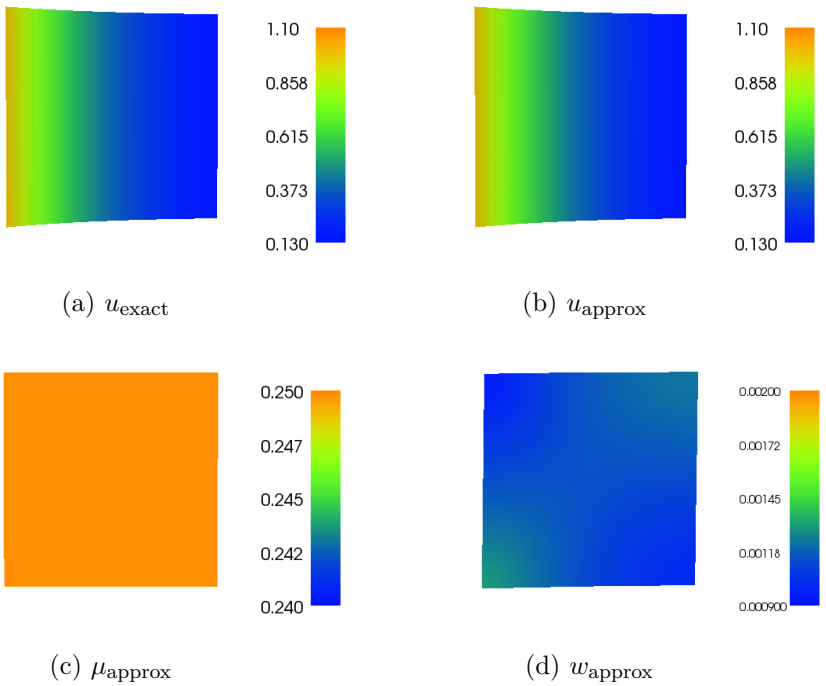

(a) u_{exact} (b) u_{approx}

(c) μ_{approx} (d) w_{approx}

Figure 4.2: Plots of the analytical and numerical solutions of u and the numerical solutions of μ and w for $\mu \in \mathbb{R}$, $\mu_{\text{prior}} = 0$, $\alpha = 0$, $\Delta_{\text{noise}} = 0\%$ and $N = 16$.

N	$E_{0,u}$	rates	$E_{1,u}$	rates	E_{μ}	rates
8	1.888E-03		7.083E-02		4.794E-04	
16	4.779E-04	1.982	3.565E-02	0.991	1.190E-04	2.010
32	1.199E-04	1.995	1.786E-02	0.997	2.954E-05	2.011
64	3.001E-05	1.998	8.936E-03	0.999	7.358E-06	2.005
128	7.505E-06	2.000	4.469E-03	1.000	1.837E-06	2.002

Table 4.2: Convergence rates with $\alpha = 0.0$ and $\Delta_{\text{noise}} = 0.0$ when $\mu \in \mathbb{R}$ and $\mu_{\text{prior}} = \mu_{\text{exact}}$.

parameter h decreases, with the exception of when $\Delta_{\text{noise}} = 3\%$, where there is a local maximum for $h = 0.0625$ and a local minimum for $h = 0.03125$. In the case of $\Delta_{\text{noise}} = 0\%$, the error decreases at a rate of approximately 2. The error of u in H^1-norm on the other hand, are approximately equal for all values of Δ_{noise}, and it decreases linearly as h decreases. Finally, for the error in μ in L^2-norm, the results are similar to the ones for the error of u in L^2-norm, but the local minimum for $\Delta_{\text{noise}} = 3\%$ are at $h = 0.015625$ and for $\Delta_{\text{noise}} = 0.3\%$ a minimum occurs at $h = 0.03125$. For $\Delta_{\text{noise}} = 0\%$, the error decreases at a rate of approximately 2 for the largest values of h, but the rate decreases as h decreases. Similar experiments using α in the range $(10^{-8}, 10)$ yield similar results. With these configurations even with noise in the input data, the solutions are qualitatively good.

Finally, we study the regularization parameter, α, for given N and Δ_{noise}. Consider the errors in u in L^2- and H^1-norms and the errors in μ in L^2-norm for $N = 64$, which are presented in Figure 4.4. We observe that the errors in u decreases as α decreases for $\alpha = 10, 1, 10^{-1}, \cdots, 10^{-8}$ for all Δ_{noise}, with the exception of $\Delta_{\text{noise}} = 0.01$, where a local minimum occurs at $\alpha = 10^{-4}$. The same is observed for the errors in μ, except here there are two local minima - one at $\alpha = 10^{-5}$ for $\Delta_{\text{noise}} = 0.03$ and the other one at $\alpha = 10^{-4}$ for $\Delta_{\text{noise}} = 0.01$. In general; lower noise yields lower errors, with the exception of no noise which has a slightly larger error than with $\Delta_{\text{noise}} = 0.003$ when α is less than 10^{-3}. Similar experiments using $N = 8, 16, 32, 128$ yield similar results.

4.2.2 Minimization with homogeneous material with prior knowledge

Consider $\mu_{\text{prior}} = \mu_{\text{exact}}$. We start by studying the case where $\alpha = 0.0$ and $\Delta_{\text{noise}} = 0\%$. The results of convergence tests are presented in Table 4.2 and the solutions are shown in Figure 4.5. We observe that we get equal results as when $\mu_{\text{prior}} = 0$.

As for the studies without prior knowledge we move on to study the affect

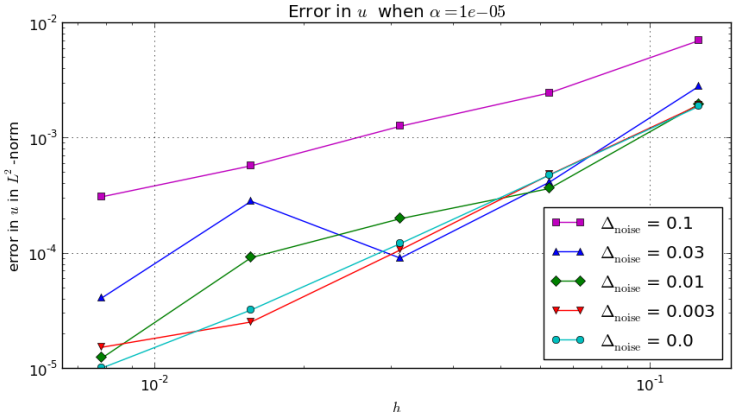

(a) The errors in u in L^2-norm

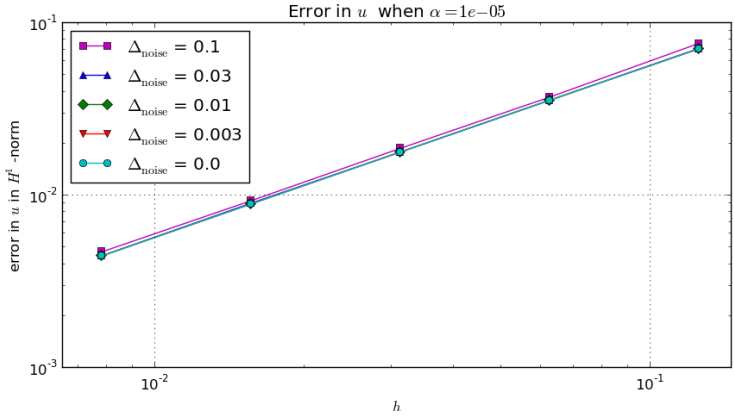

(b) The errors in u in H^1-norm

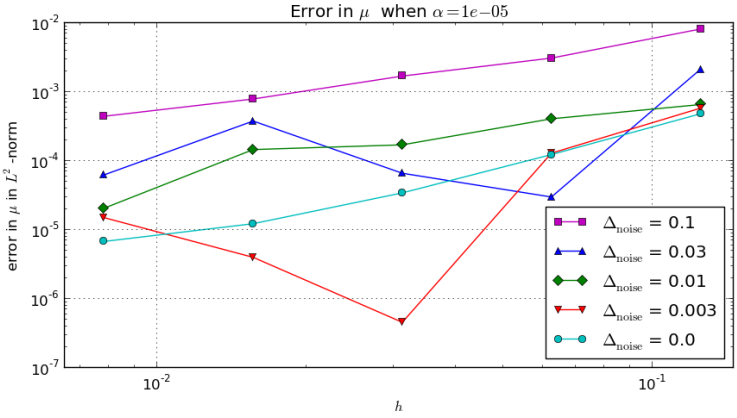

(c) The errors in μ in L^2-norm

Figure 4.3: Logarithmic plot of the errors of u in L^2- and H^1-norms and the errors of μ in L^2 norm, respectively, with $\alpha = 10^{-5}$ and with varying noise in u_{MR} when $\mu \in \mathbb{R}$ and $\mu_{\text{prior}} = 0$ for $N = 8, 16, 32, 64, 128$. h is the discretization parameter defined by $h = 1/N$.

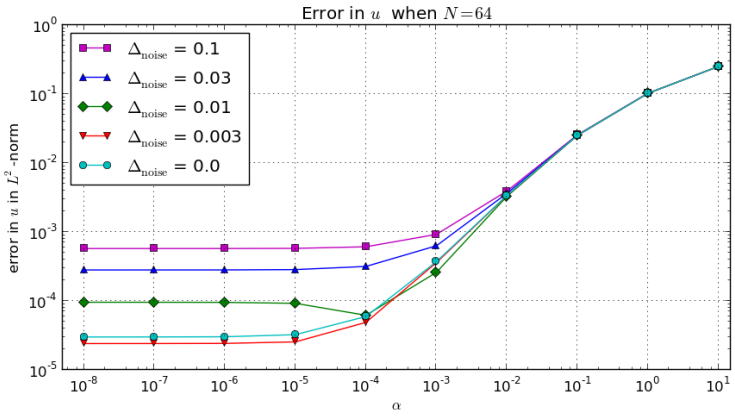

(a) The errors in u in L^2-norm

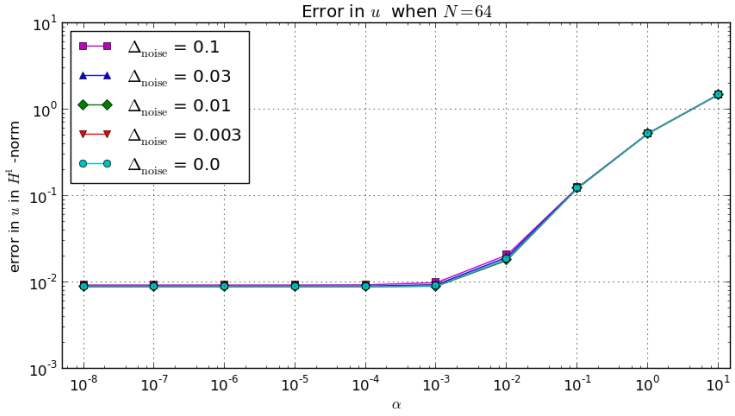

(b) The errors in u in H^1-norm

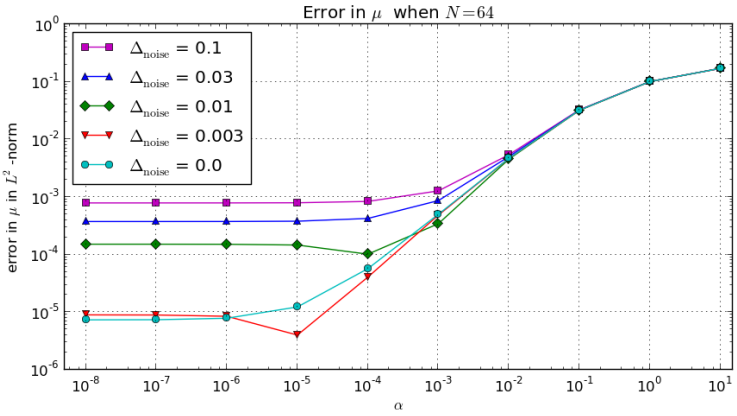

(c) The errors in μ in L^2-norm

Figure 4.4: Logarithmic plot of the errors in u in L^2- and H^1-norms and the errors in μ in L^2 norm, respectively, on a mesh of size 64×64 with varying noise in u_{MR} and α-values from 10^{-8} to 10^1 when $\mu \in \mathbb{R}$ and $\mu_{\text{prior}} = 0$.

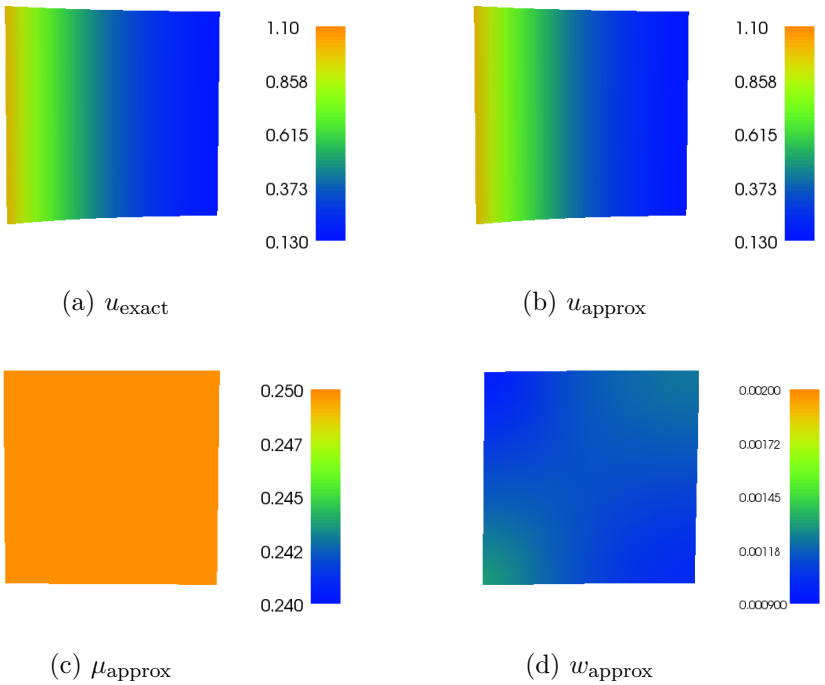

(a) u_{exact} (b) u_{approx}

(c) μ_{approx} (d) w_{approx}

Figure 4.5: Plots of the analytical and numerical solutions of u and the numerical solutions of μ and w for $\mu \in \mathbb{R}$, $\mu_{\text{prior}} = \mu_{\text{exact}}$, $\alpha = 0$, $\Delta_{\text{noise}} = 0\%$ and $N = 16$.

N	$E_{0,u}$	rates	$E_{1,u}$	rates	E_μ	rates
8	1.697E-03		7.130E-02		3.695E-03	
16	4.291E-04	1.984	3.573E-02	0.997	1.335E-03	1.469
32	1.114E-04	1.945	1.795E-02	0.994	1.430E-03	−0.099
64	3.860E-05	1.530	9.511E-03	0.916	2.648E-03	−0.889
128	-	-	-	-	-	-

Table 4.3: Convergence rates with $\alpha = 10^{-5}$ and $\Delta_{\text{noise}} = 0.0$ when $\mu \in \text{DG}_0$ and $\mu_{\text{prior}} = 0$. With $N = 128$ the Newton solver did not converge, thus no solution was obtained for u and μ in this case.

of noise in the input data. Consider the case where $\alpha = 10^{-5}$ with varying amount of noise in u_{MR}. The results are presented in Figure 4.6. Compared to the results when $\mu_{\text{prior}} = 0$, shown in Figure 4.3, we see that the results are very similar.

Finally, study of the regularization parameter, α, for given N and Δ_{noise}. Consider results for various regularization parameters for given N and given Δ_{noise}. Figure 4.7 present the results of the experiments. As for when $\mu_{\text{prior}} = 0$, the errors are stable for the smallest α-values. Different from the case when $\mu_{\text{prior}} = 0$, we observe here that the errors decrease as $\alpha > 10^2$. In general when $\mu_{\text{prior}} = \mu_{\text{exact}}$ errors are less sensitive to the value of the regularization parameter than for the case with $\mu_{\text{prior}} = 0$.

4.2.3 Minimization with heterogeneous material

As for the experiments with homogeneous material, minimization are carried out both with and without prior knowledge.

Experiments with no regularization, that is $\alpha = 0$, the Newton solver did not converge, independent of the level of noise in u_{MR}. Thus, regularization is needed for the solver to converge, when searching for $\mu \in \text{DG}_0$.

Letting $\alpha = 10^{-8}$ and $\Delta_{\text{noise}} = 0\%$, the solver converges in all of the tested configurations, using mesh sizes $N = 8, 16, 32, 64$, but does not converge when $N = 128$. In the Tables 4.3 and 4.4 the convergence rates from experiments with $\alpha = 10^{-5}$ and $\Delta_{\text{noise}} = 0.0$ are presented for $\mu_{\text{prior}} = 0$ and $\mu_{\text{prior}} = \mu_{\text{exact}}$, respectively. We observe that the rates are optimal in the case of $\mu_{\text{prior}} = \mu_{\text{exact}}$. In the case $\mu_{\text{prior}} = 0$, the rates are suboptimal and the Newton solver does not even converge for $N = 128$.

Computing the average of the components, μ_i, of the computed μ, we observe that that it is close to the exact solution in all of the acquired results. This is presented in the Tables 4.5 and 4.6 for $\mu_{\text{prior}} = 0$ and $\mu_{\text{prior}} = \mu_{\text{exact}}$, respectively, when $\alpha = 10^{-5}$ and $\Delta_{\text{noise}} = 0.0$. Figure 4.8 shows both the

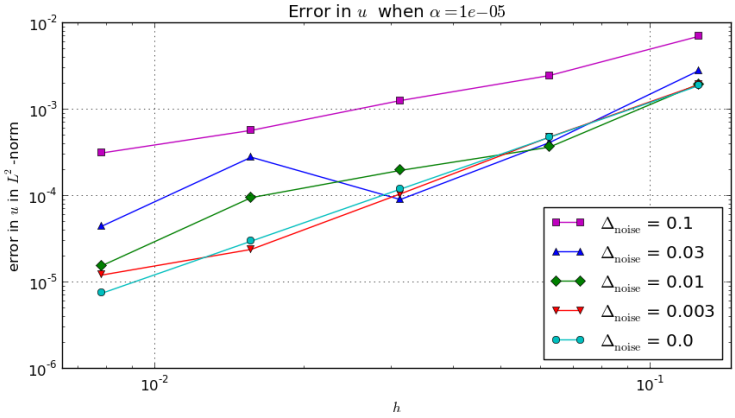

(a) The errors in u in L^2-norm

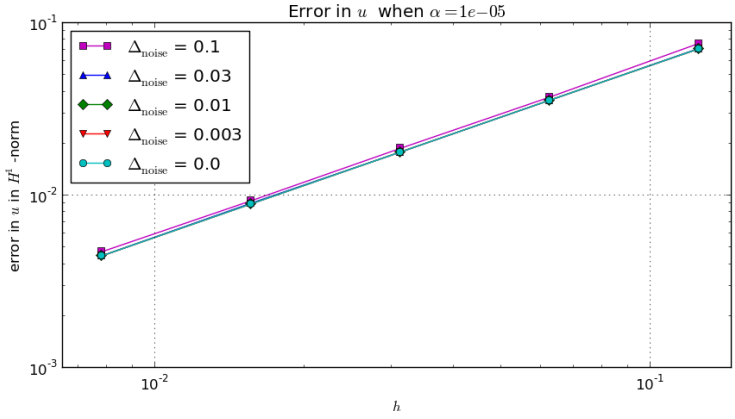

(b) The errors in u in H^1-norm

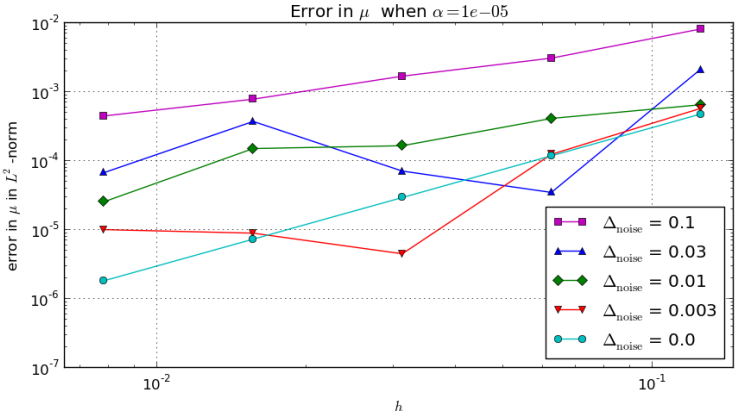

(c) The errors in μ in L^2-norm

Figure 4.6: Logarithmic plot of the errors of u in L^2- and H^1-norms and the errors of μ in L^2 norm, respectively, with $\alpha = 10^{-5}$ and with varying noise in u_{MR} when $\mu \in \mathbb{R}$ and $\mu_{\text{prior}} = \mu_{\text{exact}}$ for $N = 8, 16, 32, 64, 128$. h is the discretization parameter defined by $h = 1/N$.

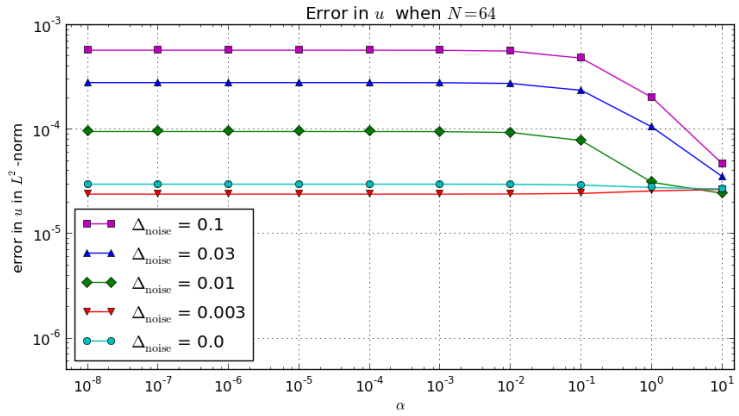

(a) The errors in u in L^2-norm

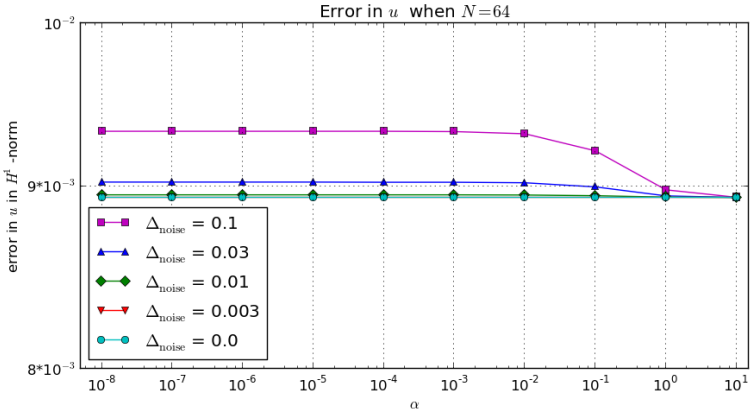

(b) The errors in u in H^1-norm

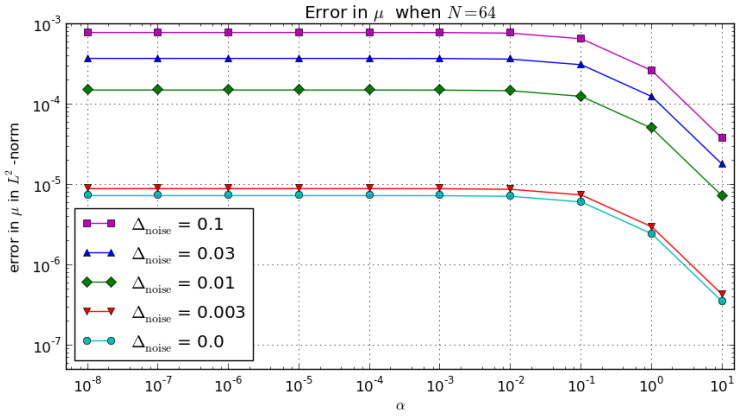

(c) The errors in μ in L^2-norm

Figure 4.7: Logarithmic plot of the errors in u in L^2- and H^1-norms and the errors in μ in L^2 norm, respectively, on a mesh of size 64×64 with varying noise in u_{MR} and α-values from 10^{-8} to 10^1 when $\mu \in \mathbb{R}$ and $\mu_{\text{prior}} = \mu_{\text{exact}}$.

N	$E_{0,u}$	rates	$E_{1,u}$	rates	E_μ	rates
8	1.695E-03		7.130E-02		3.682E-03	
16	4.262E-04	1.991	3.573E-02	0.997	1.199E-03	1.619
32	1.067E-04	1.998	1.787E-02	0.999	3.351E-04	1.839
64	2.669E-05	1.999	8.938E-03	1.000	8.828E-05	1.924
128	6.673E-06	2.000	4.469E-03	1.000	2.257E-05	1.967

Table 4.4: Convergence rates with $\alpha = 10^{-5}$ and $\Delta_{\text{noise}} = 0.0$ when $\mu \in \text{DG}_0$ and $\mu_{\text{prior}} = \mu_{\text{exact}}$.

N	μ_{avg}	SD_μ	MD_μ
8	0.2495	0.0037	0.0109
16	0.2498	0.0013	0.0081
32	0.2498	0.0014	0.0139
64	0.2497	0.0026	0.0300
128	-	-	-

Table 4.5: The average value of the components of the calculated μ, the standard deviation and the maximum deviation, for $\alpha = 10^{-5}$ and $\Delta_{\text{noise}} = 0.0$ when $\mu \in \text{DG}_0$ and $\mu_{\text{prior}} = 0$. The exact value of μ is $\mu_{\text{exact}} = 0.25$.

analytical and numerical solutions of u and the numerical solutions of μ and w when $\mu_{\text{prior}} = 0$. Figure 4.9 shows the solutions when $\mu_{\text{prior}} = \mu_{\text{exact}}$. The average, μ_{avg}, the standard deviation in μ, SD_μ, and the maximum deviation (MD) in μ, MD_μ, are defined by:

$$\mu_{\text{avg}} = \frac{\sum_{i=1}^{n} \mu_i}{n} \tag{4.13}$$

$$SD_\mu = \sqrt{\frac{\sum_{i=1}^{n} (\mu_i - \mu_{\text{avg}})^2}{n}}, \tag{4.14}$$

$$MD_\mu = \max_{1 \le i \le n} \text{abs}(\mu_i - \mu_{\text{avg}}), \tag{4.15}$$

here μ_i is the i-th component of the computed μ and n is the degrees of freedom in μ.

Adding noise in u_{MR}, the regularization parameter must be significantly increased for the solver to converge, using a maximum of 40 iterations, and absolute and relative tolerance 10^{-13} and 10^{-12}, respectively. In experiments with $\Delta_{\text{noise}} = 0.3\%$, the Newton solver does not converge for any of the tested α-values smaller than $\alpha = 10^{-4}$, with the exception of $N = 16$ for $\mu_{\text{prior}} = \mu_{\text{exact}}$ when $\alpha = 10^{-5}$ and $N = 16$ for $\mu_{\text{prior}} = 0$ when $\alpha = 10^{-6}$. When $\alpha = 10^{-4}$ the solver converges for $N = 8, 16, 32$ and for all tested values of N for $\mu_{\text{prior}} = \mu_{\text{exact}}$. For $\mu_{\text{prior}} = 0$ it converges for $N = 8, 16, 32, 64$, but not for $N = 128$, for the tested $\alpha \ge 10^{-4}$. The results show that

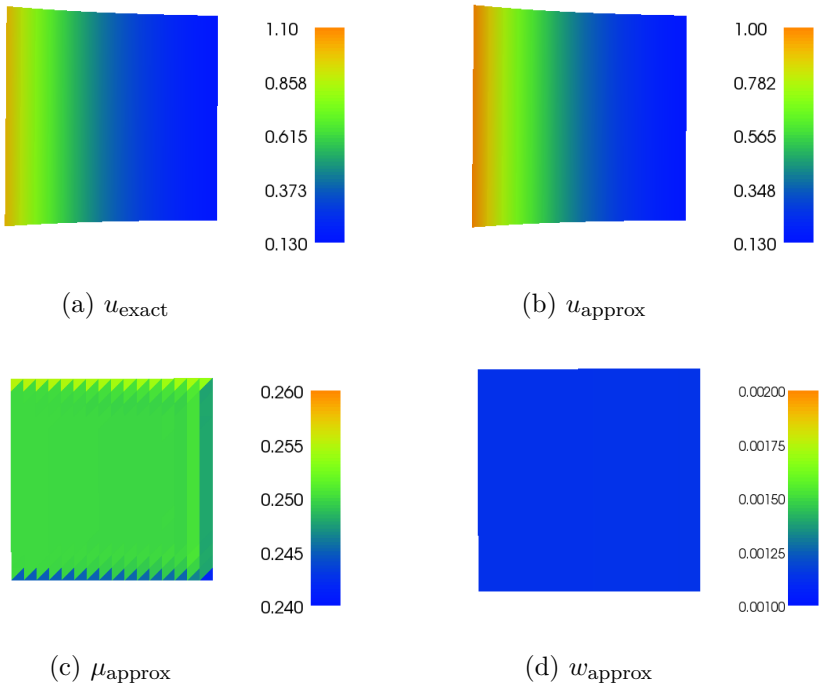

(a) u_{exact} (b) u_{approx}

(c) μ_{approx} (d) w_{approx}

Figure 4.8: Plots of the analytical and numerical solutions of u and the numerical solutions of μ and w for $\mu \in \text{DG}_0$, $\mu_{\text{prior}} = 0$, $\alpha = 10^{-5}$, $\Delta_{\text{noise}} = 0\%$ and $N = 16$.

N	μ_{avg}	SD_μ	MD_μ
8	0.2495	0.0036	0.0108
16	0.2499	0.0012	0.0053
32	0.2500	0.0003	0.0026
64	0.2500	0.0001	0.0013
128	0.2500	0.0000	0.0006

Table 4.6: The average value of the components of the calculated μ, the standard deviation and the maximum deviation, for $\alpha = 10^{-5}$ and $\Delta_{\text{noise}} = 0.0$ when $\mu \in \text{DG}_0$ and $\mu_{\text{prior}} = \mu_{\text{exact}}$. The exact value of μ is $\mu_{\text{exact}} = 0.25$.

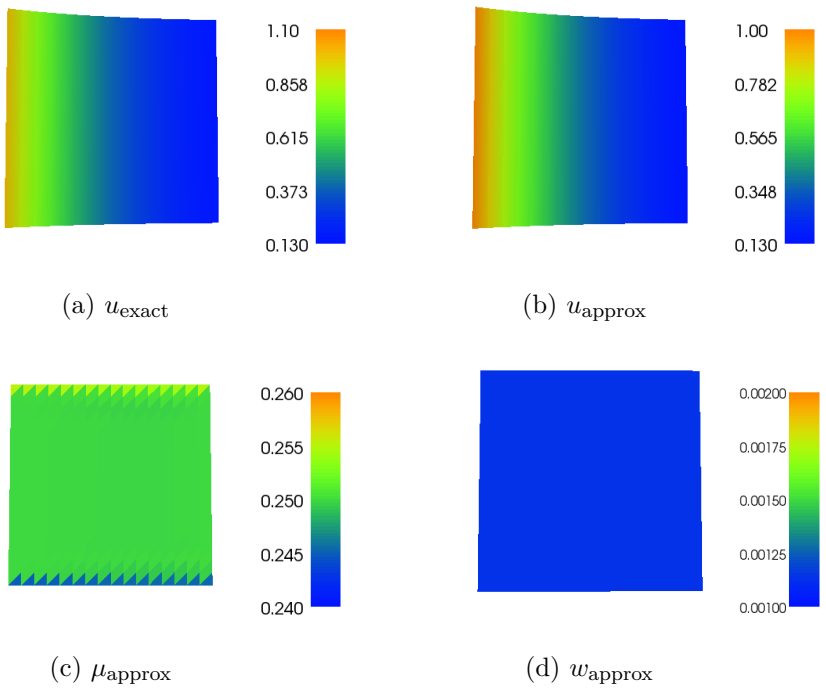

(a) u_{exact} (b) u_{approx}

(c) μ_{approx} (d) w_{approx}

Figure 4.9: Plots of the analytical and numerical solutions of u and the numerical solutions of μ and w for $\mu \in \text{DG}_0$, $\mu_{\text{prior}} = \mu_{\text{exact}}$, $\alpha = 10^{-5}$, $\Delta_{\text{noise}} = 0\%$ and $N = 16$.

as Δ_{noise} increases also α must increase for the solver to converge. When $\Delta_{\text{noise}} = 10\%$, we must have $\alpha = 0.1$ for the solver to converge. With $\alpha = 0.1$ the solver converges for the mesh sizes $N = 8, 32$ for $\mu_{\text{prior}} = 0$ and $N = 8, 16, 64, 128$ for $\mu_{\text{prior}} = \mu_{\text{exact}}$. All solvers converge, for all noise levels and all mesh sizes ($N = 8, 16, 32, 64, 128$), with $\alpha = 0.01$ when $\mu_{\text{prior}} = \mu_{\text{exact}}$. For $\mu_{\text{prior}} = 0$, the only α and Δ_{noise} the solver converge for all tested mesh sizes, are $\alpha = 1.0$ and $\Delta_{\text{noise}} = 1\%$.

As an attempt to get convergence in the Newton solver in more of the tested configurations when $\mu \in \text{DG}_0$, it has been tested with an alternative initial guess for w. Since the Newton solver converged in all of the tests with $\mu \in \mathbb{R}$, the solution of w from these tests were given as the initial guess w_0 for $\mu \in \text{DG}_0$. Unfortunately, this did not help the solver to converge in more of the experiments.

It has also been tested with lower tolerance; absolute tolerance as 10^{-10} and relative tolerance as 10^{-9} (which are the default values in FEniCS), but this did not give convergence in more of the experiments. The only improvement this change of parameters gave, was that in the experiments were solutions already were obtained fewer iterations were needed to find these solutions. Thus, in general, if the Newton solver converges, the results are qualitatively good.

4.3 Summary

The general findings from these experiments are:

- When searching for a homogeneous parameter μ, regularization is not needed to obtain qualitatively good results. However, when searching for a heterogeneous parameter μ , regularization is needed.
- When using prior knowledge the errors get smaller as the regularization parameter gets larger (which one might expect due to higher influence of the regularization term). Thus, if good target data is available it is preferable to use regularization with these data, and in the case of μ in DG_0 this improves the results and the Newton solver converges in more of the tested configurations.
- Regularization parameters $\alpha = 10^i$ for $i = -8, -7, \ldots, -4$, give qualitatively good results when μ in $\mathbb{R}$ both with and without prior knowledge for all noise levels.
- When μ is heterogeneous, the solver struggles with convergence when adding noise. $\alpha = 10^{-2}$ yields qualitatively good results for all noise levels when μ is heterogeneous and we have prior knowledge. When

μ is heterogeneous and we do not use prior knowledge, the Newton solver converges for all noise levels and all N when $\alpha = 1.0$.

The general result for noise in the measured data is; lower amount of noise yields lower errors.

Chapter 5

Study of Tikhonov regularization for the linear elasticity model

In this chapter we perform similar experiments as for the Poisson minimization problem, with the linear elasticity minimization problem. All source code used is available online at `bitbucket.org/istorpe/source-code-master-s-degree`. The code from the experiments with the Poisson model can also be found in Appendix A.

Consider the linear elasticity minimization problem given in (3.29) and (3.30): Find $(\boldsymbol{u}_h, \mu_h, \lambda_h, \boldsymbol{w}_h)$ in $V_h \times S_h \times S_h \times Q_h$ such that

$$F((\boldsymbol{u}_h, \mu_h, \lambda_h, \boldsymbol{w}_h); (\boldsymbol{v}, \eta, \kappa, \boldsymbol{q})) = 0$$

for all $(\boldsymbol{v}, \eta, \kappa, \boldsymbol{q})$ in $\hat{V}_h \times \hat{S}_h \times \hat{S}_h \times \hat{Q}_h$, where

$$F((\boldsymbol{u}_h, \mu_h, \lambda_h, \boldsymbol{w}_h); (\boldsymbol{v}, \eta, \kappa, \boldsymbol{q})) = \frac{\partial \mathcal{L}}{\partial \boldsymbol{u}_h}[\boldsymbol{v}] + \frac{\partial \mathcal{L}}{\partial \mu_h}[\eta] + \frac{\partial \mathcal{L}}{\partial \lambda_h}[\kappa] + \frac{\partial \mathcal{L}}{\partial \boldsymbol{w}_h}[\boldsymbol{q}].$$

Using this model, similar experiments as for the Poisson problem will be performed to get an understanding of the sensitivity to noise in the linear elasticity minimization problem and how regularization affects the solutions.

In stead of deriving a manufactured solution analytically as for the Poisson problem, we solve the forward problem given in (2.12) numerically with the

following input functions and domain:

$$\mu_{\text{exact}} = 3.0, \tag{5.1}$$
$$\lambda_{\text{exact}} = 8.0, \tag{5.2}$$
$$\boldsymbol{t} = (0.9, 0.3), \tag{5.3}$$
$$\Omega = [0,1] \times [0,1]. \tag{5.4}$$

to obtain a target solution for $\boldsymbol{u}$ and denote this solution $\boldsymbol{u}_{\text{exact}}$. This method to get target solutions are commonly used when solving inverse problems [10].

5.1 Experiments and results with the elasticity minimization problem

Consider the same scenarios as for the Poisson problem:

- μ, λ in $\mathbb{R}$ vs. DG_0
- Varying regualization parameters α, β
- Adding noise in u_{MR}
- $\mu_{\text{prior}} = 0, \lambda_{\text{prior}} = 0$ vs. $\mu_{\text{prior}} = \mu_{\text{exact}}, \lambda_{\text{prior}} = \lambda_{\text{exact}}$

In these experiments we want to check whether we get similar results as for the Poisson minimization problem or not.

Let u_{MR} be defined as in Eq. (4.6) and let the considered amounts of noise in u_{MR} be, as previously, $\Delta_{\text{noise}} = 10\%, 3\%, 1\%, 0.3\%$ and 0%. Also, consider the error norms studied in the Poisson problem:

$$\begin{aligned} E_{0,u} &= \|\boldsymbol{u}_{\text{exact}} - \boldsymbol{u}\|_{L^2(\Omega)}, \\ E_{1,u} &= \|\boldsymbol{u}_{\text{exact}} - \boldsymbol{u}\|_{H^1(\Omega)}, \\ E_{\mu} &= \|\mu_{\text{exact}} - \mu\|_{L^2(\Omega)}, \\ E_{\lambda} &= \|\lambda_{\text{exact}} - \lambda\|_{L^2(\Omega)}. \end{aligned} \tag{5.5}$$

The convergence rates are computed as defined in Eq. (4.11). The mesh sizes consider for the linear elasticity problem are $8 \times 8, 16 \times 16, 32 \times 32$ and 64×64. The mesh size 128×128 is not tested in this case, as this was to demanding for the computer.

In the Newton solver the absolute tolerance is 10^{-10} and the relative tolerance is 10^{-9}, which are the default values in FEniCS. The initial guesses for

N	$E_{0,u}$	rates	$E_{1,u}$	rates	E_μ	rates	E_λ	rates
8	2.50E-03		6.97E-02		6.55E-02		5.93E+00	
16	9.99E-04	1.326	4.03E-02	0.789	9.78E-03	2.745	3.26E+00	0.863
32	3.67E-04	1.445	2.26E-02	0.834	1.29E-03	2.919	1.26E+00	1.370
64	1.21E-04	1.604	1.23E-02	0.883	2.50E-04	2.371	3.70E-01	1.771

Table 5.1: Convergence rates with $\alpha = 0.0$, $\beta = 0.0$ and $\Delta_{\text{noise}} = 0.0$ when $\mu, \lambda \in \mathbb{R}$ and $\mu_{\text{prior}} = 0$ and $\lambda_{\text{prior}} = 0$.

$\boldsymbol{u}, \mu, \lambda$ and $\boldsymbol{w}$ in the Newton solver are:

$$\begin{aligned} \boldsymbol{u}_0 &= \boldsymbol{u}_{\text{exact}} \\ \mu_0 &= \mu_{\text{exact}} \\ \lambda_0 &= \lambda_{\text{exact}} \\ \boldsymbol{w}_0 &= (1.0, 1.0) \end{aligned} \tag{5.6}$$

In the following section the results from the experiments are presented.

5.1.1 Minimization with homogeneous material without prior knowledge

Consider the simplest test case, i.e. without regularization, that is $\alpha = \beta = 0$, and without noise in $\boldsymbol{u}_{\text{MR}}$, that is $\Delta_{\text{noise}} = 0$. The computed convergence rates in this case are presented in Table 5.1. The optimal values for the rates computed in L^2-norms are 2. We observe that the rates for the errors in $\boldsymbol{u}$ in L^2-norm start at 1.326 for the smallest mesh sizes, and as the mesh sizes increase, the rates increase as well. The largest rate is 1.604, so the rate gets closer to 2, but if larger mesh sizes had been tested we can speculate in that the rates would show a clearer convergence to 2. The rates for the errors in μ and λ are similar as those for $\boldsymbol{u}$ in L^2-norm, except that the rate for μ start at 2.745 and decrease as the mesh size increase and for the largest mesh sizes the rate is 2.371. For the rates for the errors in $\boldsymbol{u}$ in H^1-norm, the lowest rate is 0.789. As the mesh size is increased the rate increase, the largest rate is 0.883. The optimal convergence rate in the H^1-norm is 1. The numerical solutions for $\boldsymbol{u}, \mu, \lambda$ and $\boldsymbol{w}$ are shown in Figure 5.1.

Still let the regularization parameters equal zero and let the amount of synthetic noise in $\boldsymbol{u}_{\text{MR}}$ vary. The errors in the approximations in this case are presented in Figures 5.2 and 5.3. In all of the considered error norms, we observe that the errors in the approximations without any noise decrease as expected as the discretization parameter $h = 1/N$ decreases. When adding noise, the errors vary more and in the case of $\Delta_{\text{noise}} = 0.1$ the Newton solver only converged for $N = 32, 64$, for $\Delta_{\text{noise}} = 0.03$ the solver only converged

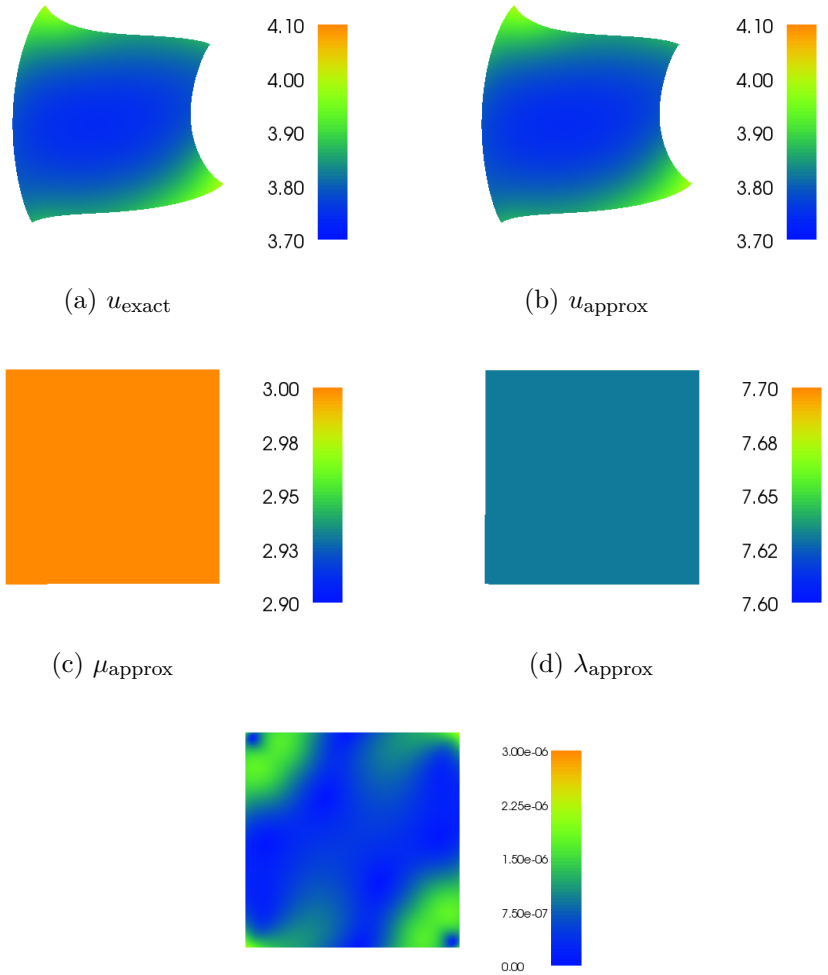

(a) u_{exact} (b) u_{approx}

(c) μ_{approx} (d) λ_{approx}

(e) w_{approx}

Figure 5.1: Plots of the analytical and numerical solutions of u and the numerical solutions of μ, λ and w for $\mu, \lambda \in \mathbb{R}$, $\mu_{\text{prior}} = 0, \lambda_{\text{prior}} = 0$, $\alpha = 0$, $\beta = 0$, $\Delta_{\text{noise}} = 0\%$ and $N = 64$.

for $N = 8, 16, 64$ and for $\Delta_{\text{noise}} = 0.01$ the solver only converged for $N = 8, 16, 32$. Firstly, consider the errors in $\boldsymbol{u}$ in L^2-norm. With 0.3% noise in $\boldsymbol{u}_{\text{MR}}$ the errors follow the errors from when $\Delta_{\text{noise}} = 0$ quite closely, with the exception of the smallest h, where it is a bit larger. For the other amounts of noise, the errors vary more, and for $\Delta_{\text{noise}} = 0.1$ it even increases for larger mesh size. Secondly, consider the errors in $\boldsymbol{u}$ in H^1-norm. Here, the errors do not vary as much as for the L^2-norm, except from when $\Delta_{\text{noise}} = 0.1$ in which the errors are larger and does not decrease for increased mesh size. Finally, consider the errors in μ and λ in L^2-norms. We observe that adding noise to $\boldsymbol{u}_{\text{MR}}$ makes the errors vary a lot, and there is clear tendency that the error decrease as the mesh size is increased. An exception is the errors in λ when $\Delta_{\text{noise}} = 0.003$, here the errors are close to the errors without noise.

Similar experiments has been carried out when letting α and β vary from $10^{-8}, 10^{-7}, \ldots, 10^{1}$ and with both $\alpha = \beta$ and $\alpha \neq \beta$. The experiments with the smallest values of α and β, that is the values 10^{-8} and 10^{-7} yield similar results as those for $\alpha = \beta = 0$. Increasing α and β makes the errors more and more equal and the error is the about the same for all mesh sizes, that is, for large regularization parameters the errors do not decrease as the mesh size is increased.

Finally, we study the affect of the regularization parameters, α and β. Consider the errors in the numerical solutions for $N = 64$ and various amounts of noise in $\boldsymbol{u}_{\text{MR}}$, which are presented in Figure 5.4. We observe that the general tendency in these plots are that the errors increase as the regularization parameters increase. The exceptions are the errors in λ in L^2-norm which stay stable for regularization values larger than 10^{-6}. For the errors in μ in L^2-norm, a local minimum is observed for Δ_{noise} for $\alpha = \beta = 10^{-4}$. All the Δ_{noise}-values except $\Delta_{\text{noise}} = 0.1$, yield a local maximum for $\alpha = \beta = 10^{-1}$ for the errors in $\boldsymbol{u}$ in H^1-norm. Similar experiments for the mesh sizes with $N = 8, 16, 32$ yield similar results.

5.1.2 Minimization with homogeneous material with prior knowledge

As for the case when $\mu_{\text{prior}} = \lambda_{\text{prior}} = 0$, consider the configuration $\alpha = \beta = 0$ and $\Delta_{\text{noise}} = 0$. As expected, the convergence rates are equal to those computed for when $\mu_{\text{prior}} = \lambda_{\text{prior}} = 0$. The rates are presented in Table 5.2 and the plots of the solution functions are shown in Figure 5.5.

Study the configuration using $\alpha = \beta = 10^{-3}$ and various amounts of noise in $\boldsymbol{u}_{\text{MR}}$. The errors in the approximations from this setup are shown in Figures 5.6 and 5.7 and using this regularization the Newton solver converges for

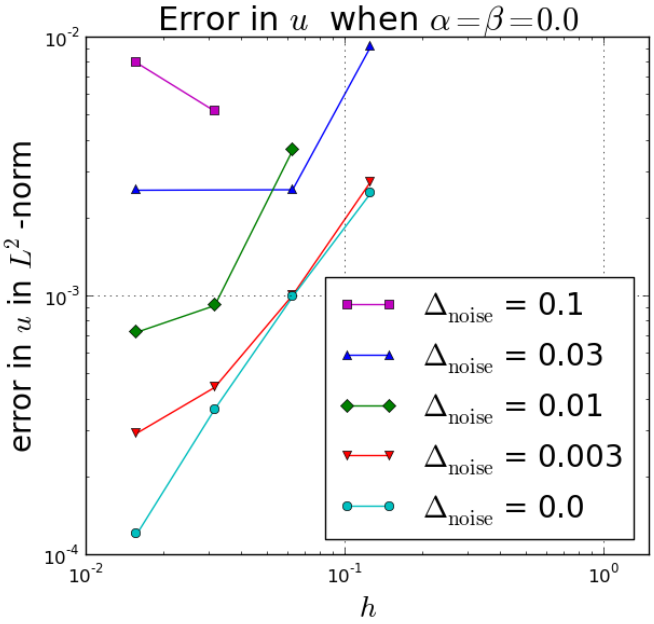

(a) The errors in u in L^2-norm

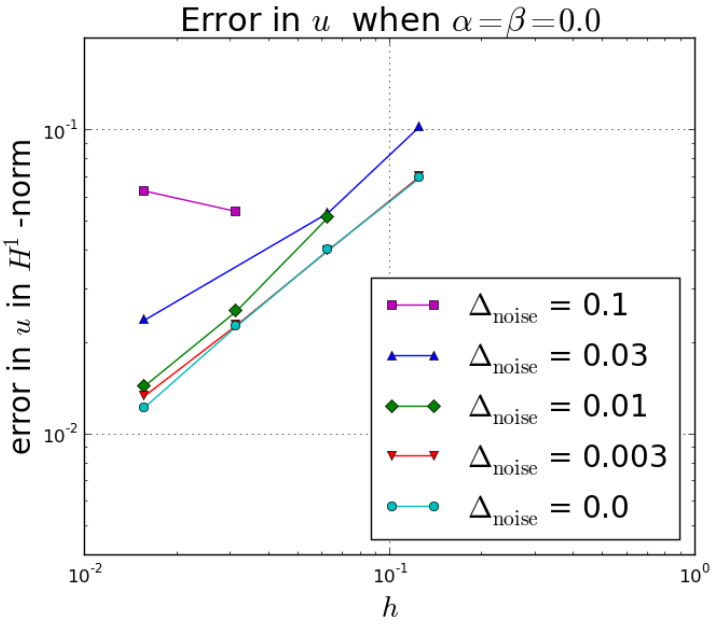

(b) The errors in u in H^1-norm

Figure 5.2: Logarithmic plot of the errors in u in L^2- and H^1-norms, respectively, when $\mu, \lambda \in \mathbb{R}$ and $\mu_{\text{prior}} = 0$ and $\lambda_{\text{prior}} = 0$ for $N = 8, 16, 32, 64$. The regularization parameters $\alpha = \beta = 0.0$ and with varying noise in u_{MR}. h is the discretization parameter defined by $h = 1/N$.

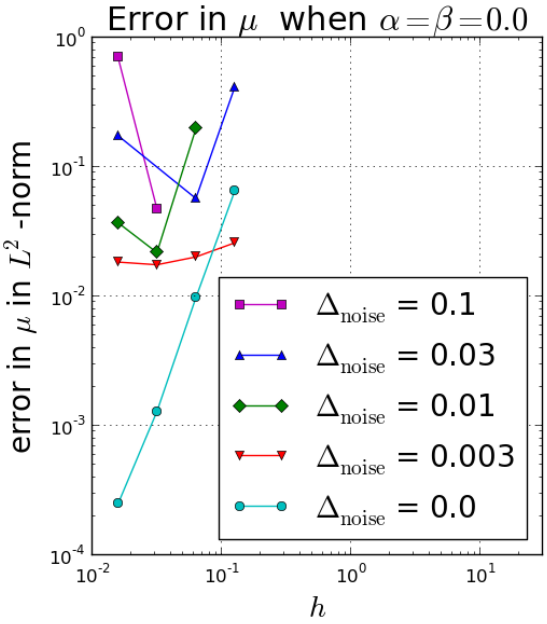

(a) The errors in μ in L^2-norm

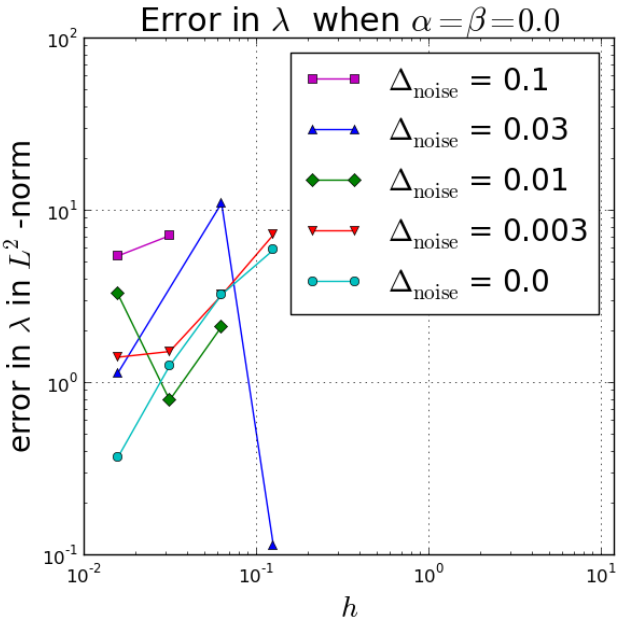

(b) The errors in λ in L^2-norm

Figure 5.3: Logarithmic plot of the errors in μ and λ in L^2 norm, respectively, when $\mu, \lambda \in \mathbb{R}$ and $\mu_{\text{prior}} = 0$ and $\lambda_{\text{prior}} = 0$ for $N = 8, 16, 32, 64$. The regularization parameters $\alpha = \beta = 0.0$ and with varying noise in u_{MR}. h is the discretization parameter defined by $h = 1/N$.

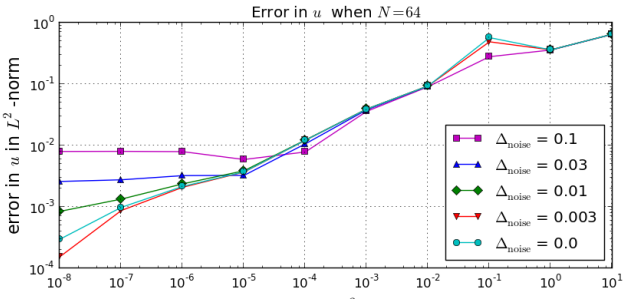

(a) The errors in u in L^2-norm

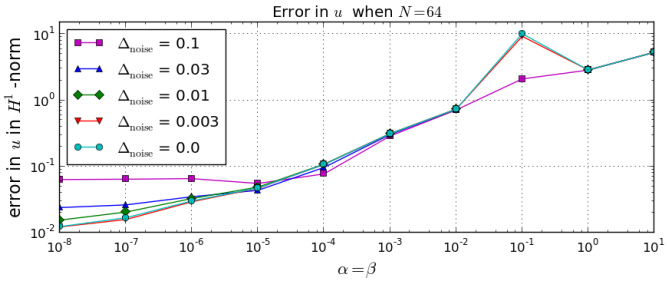

(b) The errors in u in H^1-norm

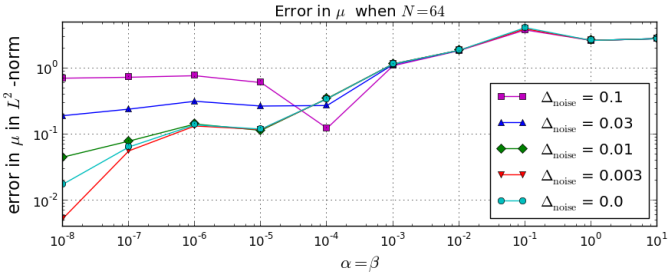

(c) The errors in μ in L^2-norm

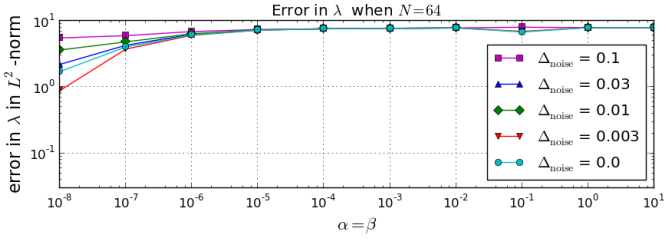

(d) The errors in λ in L^2-norm

Figure 5.4: Logarithmic plot of the errors in u in L^2- and H^1-norms and the errors in μ and λ in L^2 norm, respectively, on a mesh of size 64×64 with varying noise in u_{MR} and equal regularization parameters $\alpha = \beta$ with values from 10^{-8} to 10^{1} when $\mu, \lambda \in \mathbb{R}$ and $\mu_{\text{prior}} = 0$ and $\lambda_{\text{prior}} = 0$.

N	$E_{0,u}$	rates	$E_{1,u}$	rates	E_{μ}	rates	E_{λ}	rates
8	2.50E-03		6.99E-02		6.55E-02		5.93E+00	
16	9.99E-04	1.326	4.03E-02	0.789	9.78E-03	2.745	3.26E+00	0.863
32	3.67E-04	1.445	2.26E-02	0.834	1.29E-03	2.919	1.26E+00	1.370
64	1.21E-04	1.604	1.23E-02	0.883	2.50E-04	2.371	3.70E-01	1.771

Table 5.2: Convergence rates with $\alpha = 0.0$, $\beta = 0.0$ and $\Delta_{\text{noise}} = 0.0$ when $\mu, \lambda \in \mathbb{R}$ and $\mu_{\text{prior}} = \mu_{\text{exact}}$ and $\lambda_{\text{prior}} = \lambda_{\text{exact}}$.

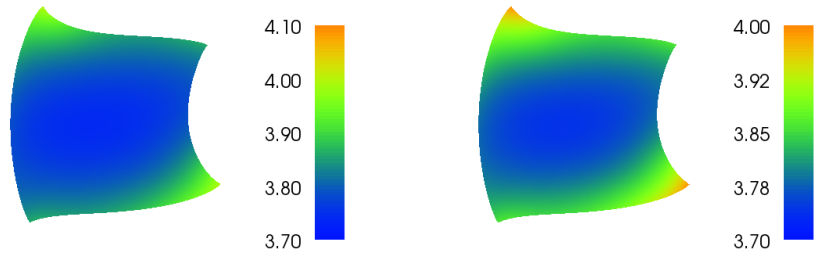

(a) u_{exact}

(b) u_{approx}

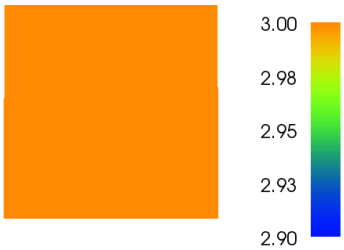

(c) μ_{approx}

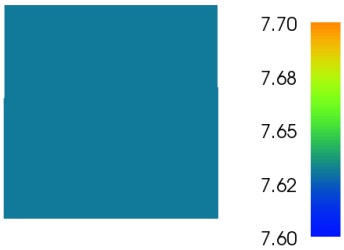

(d) λ_{approx}

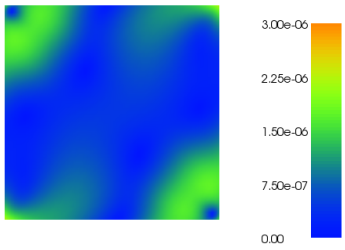

(e) w_{approx}

Figure 5.5: Plots of the analytical and numerical solutions of u and the numerical solutions of μ, λ and w for $\mu, \lambda \in \mathbb{R}$, $\mu_{\text{prior}} = \mu_{\text{exact}}, \lambda_{\text{prior}} = \lambda_{\text{exact}}$, $\alpha = 0, \beta = 0$, $\Delta_{\text{noise}} = 0\%$ and $N = 64$.

all the noise levels and all mesh sizes. The errors in the approximations without noise in $\boldsymbol{u}_{\text{MR}}$ are similar to those presented in Figures 5.2 and 5.3 and decrease as the mesh sizes increase. The errors in $\boldsymbol{u}$ in L^2-norm are quite similar for the noise amounts $\Delta_{\text{noise}} = 0.03, 0.01, 0.003, 0.0$, except for the mesh size where $N = 64$, for which the error when $\Delta_{\text{noise}} = 0.03$ is a bit larger. When $\Delta_{\text{noise}} = 0.1$, the there is a local minimum for $h = 1/32$ and the errors vary quite a lot. The errors in $\boldsymbol{u}$ in H^1-norm are almost equal independent of the amount of noise in $\boldsymbol{u}_{\text{MR}}$, with the exception when $\Delta_{\text{noise}} = 0.1$, where the errors are slightly larger for $h = 1/64$ and $h = 1/16$. For μ, the errors vary a lot for the two largest Δ_{noise}-values. When $\Delta_{\text{noise}} = 0.1$ there is a local minimum when $h = 1/32$ and for $\Delta_{\text{noise}} = 0.03$ there is a minimum for $h = 1/16$. The errors when $\Delta_{\text{noise}} = 0.01, 0.003$ are close to the errors when $\Delta_{\text{noise}} = 0.0$, with the exception of a minimum for $\Delta_{\text{noise}} = 0.003$ when $h = 1/32$. Finally, considering the errors in λ, we observe that all errors decrease as the mesh size increase, except from when $\Delta_{\text{noise}} = 0.1$ where there is a minimum for $h = 1/8$ and when $\Delta_{\text{noise}} = 0.03, 0.01$ which have minima at $h = 1/32$. Similar experiments using $\alpha, \beta = 10^{-8}, 10^{-7}, \ldots, 10^{1}$ both for $\alpha = \beta$ and $\alpha \neq \beta$ yield similar results.

Finally, study the regularization parameters α and β for given N and various Δ_{noise}. Figure 5.8 presents the errors in the approximations on the mesh size with $N = 64$. Comparing these results to the results in Figure 5.4, we observe that regularization has opposite effect when we have prior knowledge than without prior knowledge. For all noise levels in the case $\mu_{\text{prior}} = \mu_{\text{exact}}$ and $\lambda_{\text{prior}} = \lambda_{\text{exact}}$ the errors decrease or remain the same with increased values of regularization parameters, with the exception of a local minimum for the errors in μ, which have a local minimum for $\alpha = \beta = 10^{-7}$. Similar results for the mesh sizes with $N = 8, 16, 32$ yield similar results.

5.1.3 Minimization with heterogeneous material without prior knowledge

Let the setup be the same as previously, but in stead of searching for $\mu, \lambda \in \mathbb{R}$, let $\mu, \lambda \in \text{DG}_0$, that is the material are heterogeneous in stead of homogeneous. The experiments show that in this case, independent of Δ_{noise}, regularization is needed. Without regularization when $\mu, \lambda \in \text{DG}_0$, the Newton solver diverges.

Consider the case with $\mu_{\text{prior}} = \lambda_{\text{prior}} = 0$. Independent of regularization and noise, experiments show that with these guesses for the Lamé parameters the Newton solver only converge for the two smallest mesh sizes tested, that is using $N = 8, 16$. Letting the noise in $\boldsymbol{u}_{\text{MR}}$ be $10\%, 3\%, 1\%, 0.3\%$ and 0%, experiments show that when $\Delta_{\text{noise}} = 0.1$ the Newton solver only converge for the combination $\alpha = 0.001$ and $\beta = 0.001, 0.01, \ldots, 10$. The obtained

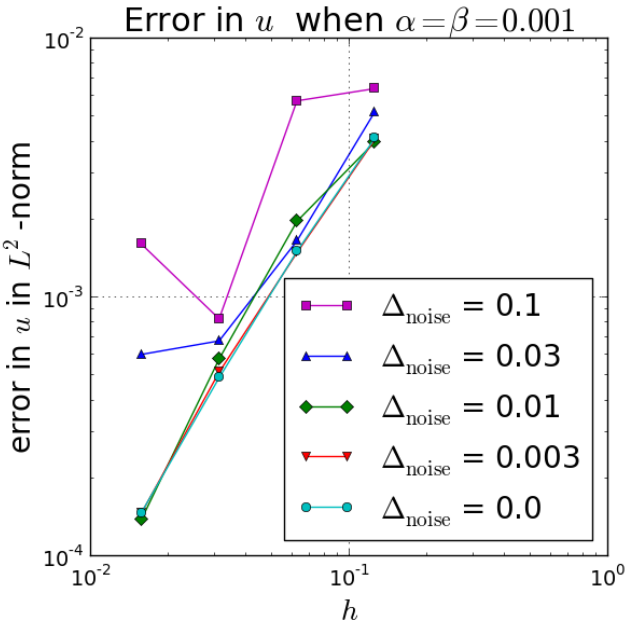

(a) The errors in u in L^2-norm

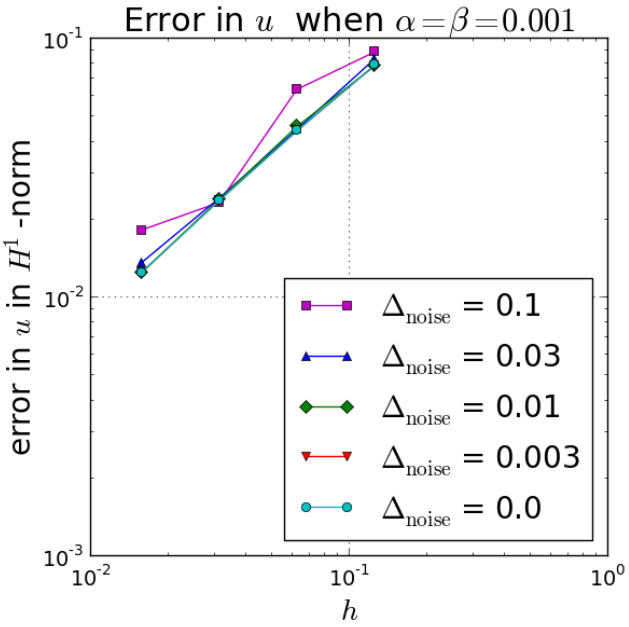

(b) The errors in u in H^1-norm

Figure 5.6: Logarithmic plot of the errors in u in L^2- and H^1-norms, respectively, with $\alpha = 10^{-3}$ and $\beta = 10^{-3}$ and with varying noise in u_{MR} when $\mu, \lambda \in \mathbb{R}$ and $\mu_{\text{prior}} = \mu_{\text{exact}}$ and $\lambda_{\text{prior}} = \lambda_{\text{exact}}$.

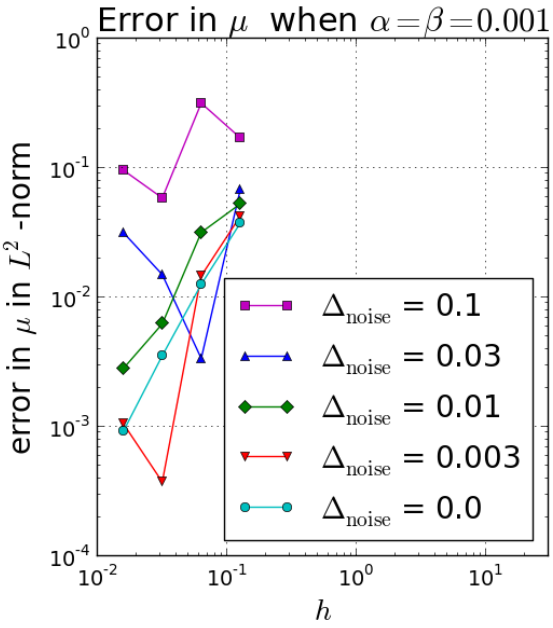

(a) The errors in μ in L^2-norm

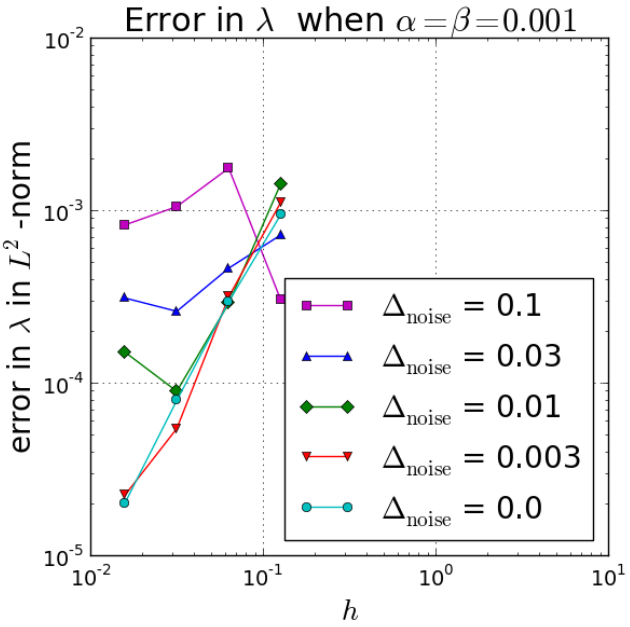

(b) The errors in λ in L^2-norm

Figure 5.7: Logarithmic plot of the errors in μ and λ in L^2 norm, respectively, with $\alpha = 10^{-3}$ and $\beta = 10^{-3}$ and with varying noise in u_{MR} when $\mu, \lambda \in \mathbb{R}$ and $\mu_{\text{prior}} = \mu_{\text{exact}}$ and $\lambda_{\text{prior}} = \lambda_{\text{exact}}$.

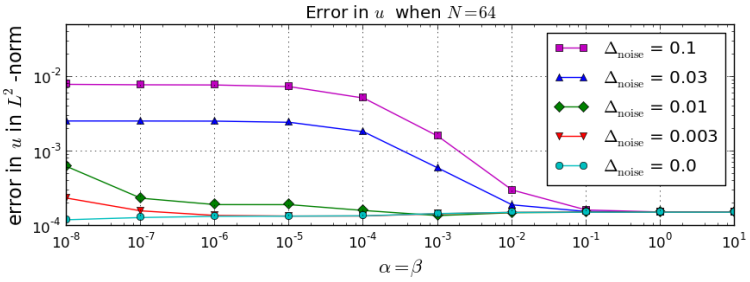

(a) The errors in u in L^2-norm

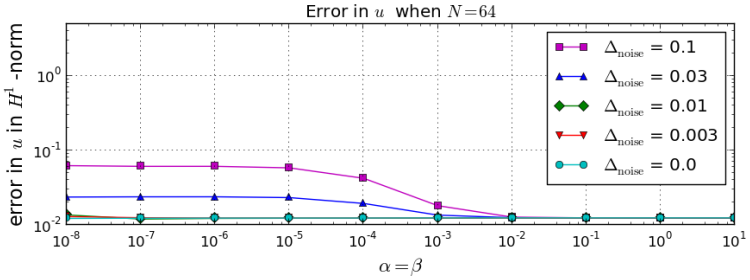

(b) The errors in u in H^1-norm

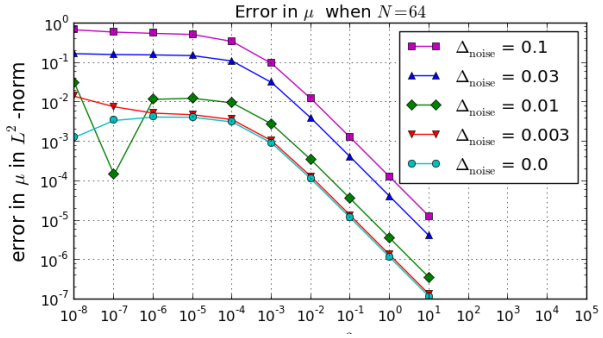

(c) The errors in μ in L^2-norm

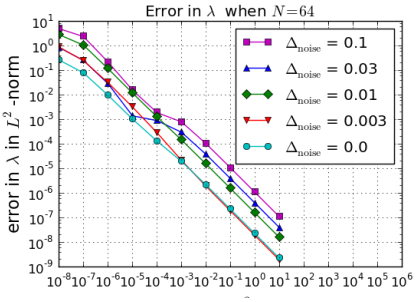

(d) The errors in λ in L^2-norm

Figure 5.8: Logarithmic plot of the errors in u in L^2- and H^1-norms and the errors in μ and λ in L^2 norm, respectively, on a mesh of size 64×64 with varying noise in u_{MR} and equal regularization parameters $\alpha = \beta$ with values from 10^{-8} to 10^{1} when $\mu, \lambda \in \mathbb{R}$ and $\mu_{\text{prior}} = \mu_{\text{prior}}$ and $\lambda_{\text{prior}} = \lambda_{\text{prior}}$.

N	$E_{0,u}$	rates	$E_{1,u}$	rates	E_μ	rates	E_λ	rates
8	3.931E-03		7.827E-02		4.522E-02		2.375E-03	
16	1.434E-03	1.455	4.372E-02	0.840	1.575E-02	1.522	6.883E-04	1.787
32	4.678E-04	1.616	2.352E-02	0.894	4.626E-03	1.767	1.752E-04	1.974
64	1.416E-04	1.724	1.244E-02	0.919	1.247E-03	1.891	4.248E-05	2.044

Table 5.3: Convergence rates with $\alpha = 10^{-3}$, $\beta = 10^{-3}$ and $\Delta_{\text{noise}} = 0.0$ when $\mu, \lambda \in \text{DG}_0$ and $\mu_{\text{prior}} = \mu_{\text{exact}}$ and $\lambda_{\text{prior}} = \lambda_{\text{exact}}$.

solutions with this regularization are quite far from the exact solutions, e.g. when $\alpha = 0.001$, $\beta = 0.1$ and $N = 16$ the obtained solutions for the Lamé parameters are $\mu_{\text{approx}} = 1.598$ and $\lambda_{\text{approx}} = 0.0001$. Recall that the exact solutions are $\mu_{\text{exact}} = 3.0$ and $\lambda_{\text{exact}} = 8.0$. When adding less amounts of noise to $\boldsymbol{u}_{\text{MR}}$ the Newton solver converges for more of the tested combinations for the regularization parameters. With no noise in $\boldsymbol{u}_{\text{MR}}$, the Newton solver converges for the values in the range $\alpha = 10^{-7}, 10^{-6}, \ldots, 10^{-3}$ and $\beta = 10^{-6}, 10^{-5}, \ldots, 10^{-1}$. The solutions obtained with these regularization parameters are similar to the example given for $\Delta_{\text{noise}} = 0.1$.

5.1.4 Minimization with heterogeneous material with prior knowledge

For equal regularization parameters the Newton solver converges only for the values $\alpha = \beta = 10^{-3}, 10^{-2}$. With these parameters the solver for all the tested mesh sizes and all tested noise levels, with the exception of when $\alpha = \beta = 10^{-3}$ it does not converge for any N when $\Delta_{\text{noise}} = 0.1$, and for $\Delta_{\text{noise}} = 0.03$ it only converges for $N = 8, 16$. Letting $\alpha \neq \beta$, the Newton solver converges for several of the combinations with α and β in the range $\{10^{-6}, 10^{-5}, \ldots, 10\}$.

Consider the case where $\alpha = \beta = 10^{-3}$ and $\Delta_{\text{noise}} = 0$. Convergence rates from this case are computed and presented in Table 5.3. We observe as expected that the errors in L^2-norm converge to 2, and the errors H^1-norm converge to 1. For $N = 64$, the computed solutions are shown in Figure 5.9. As for the Poisson equation, consider the average, standard deviation and maximum deviation in the computed approximations of the Lamé parameters, which is presented in Table 5.4 for $\alpha = \beta = 10^{-3}$. The definition of these quantities are given in (4.13). We observe that the computed solutions are very close to the exact solutions and the deviations in the solutions are small. The other regularization parameters where the Newton solver converge yield similar results.

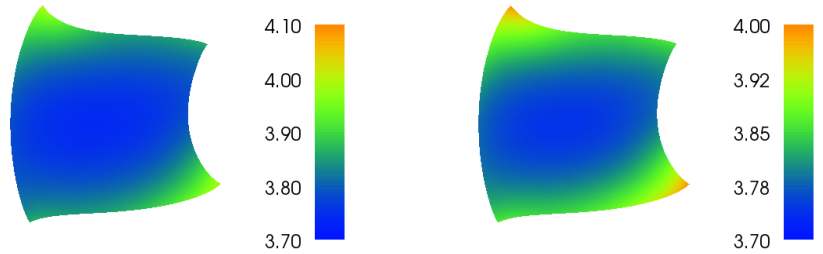

(a) u_{exact}

(b) u_{approx}

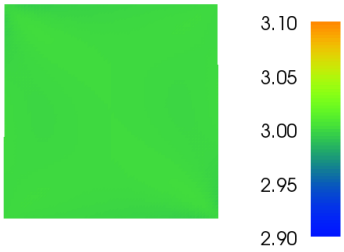

(c) μ_{approx}

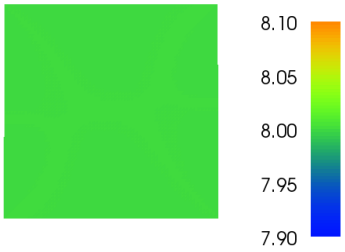

(d) λ_{approx}

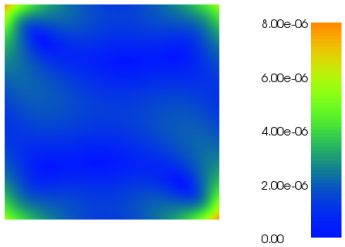

(e) w_{approx}

Figure 5.9: Plots of the analytical and numerical solutions of u and the numerical solutions of μ, λ and w for $\mu, \lambda \in \text{DG}_0$, $\mu_{\text{prior}} = \mu_{\text{exact}}, \lambda_{\text{prior}} = \lambda_{\text{exact}}$, $\alpha = 10^{-3}, \beta = 10^{-3}$, $\Delta_{\text{noise}} = 0\%$ and $N = 64$.

N	μ_{avg}	SD_μ	MD_μ	λ_{avg}	SD_λ	MD_λ
8	2.965	0.029	0.097	7.999	0.002	0.010
16	2.989	0.011	0.039	8.000	0.001	0.003
32	2.997	0.003	0.014	8.000	0.000	0.001
64	2.999	0.001	0.005	8.000	0.000	0.000

Table 5.4: The average value of the components of the calculated μ and λ, the standard deviation and the maximum deviation, for $\alpha = 10^{-3}$, $\beta = 10^{-3}$ and $\Delta_{\text{noise}} = 0.0$ when $\mu, \lambda \in \text{DG}_0$ and $\mu_{\text{prior}} = \mu_{\text{exact}}$ and $\lambda_{\text{prior}} = \lambda_{\text{exact}}$. The exact values are $\mu_{\text{exact}} = 3.0$ and $\lambda_{\text{exact}} = 8.0$.

5.2 Summary

The general findings in the experiments done with the linear elasticity model are similar to those found for the Poisson problem. However, the findings were clearer in the Poisson problem and the solver struggles more with convergence in the experiments with heterogeneous material in the elasticity problem. The results in the elasticity experiments varies more, and with more than 1% synthetic noise in the target data, the rates of the errors did not converge. The general findings for the linear elasticity minimization problem are:

- In this model, as for the Poisson model, regularization yields great improvement when the target data is good.
- When the target data is far from the exact solutions, regularization aggravates the results. Nevertheless, using regularization parameters in the range 10^{-7} to 10^{-4} yield fairly good results for homogeneous parameters in experiments both with and without prior knowledge.
- However, when μ, λ are heterogeneous, more regularization is required to obtain satisfactory solutions. In this case $\alpha = \beta = 10^{-3}$ yield good results, both with and without prior knowledge.

Chapter 6

Qualitative experiments with liver data

In the following experiments, data from MRE of a healthy liver will be used to try to decide the shear modulus of said liver. The acquired MRE data for the following experiments are from a healthy individual and the MR images are taken as horizontal cross sections through the body in the area were the liver is located. Figure 6.1a shows the MRE image and the anatomy of the body. Observe that the image shows the whole cross section of the body. The two objects on the sides in the picture, are the arms of the volunteer. The spinal cord is in the centre of the image, the liver is on the left hand side and the stomach is to the lower right. A wave map, visualizing how the wave is transmitted within the tissue, and the shear modulus is computed using the software MRE/Wave [11] provided by the Mayo Clinic. This preprocessing was already done by Karen Støverud before the work of this thesis started and the results are presented in Figures 6.1b and 6.1c. Note that the shear modulus varies from 0 kPa to 8 kPa. The area with the largest shear stiffness, where the color is red and yellow, is the stomach. The yellow boxes in the images illustrate the area of consideration in the following experiments. This area is located inside the liver.

All source code used is available online at
`bitbucket.org/istorpe/source-code-master-s-degree`. The code from the experiments with the Poisson model can also be found in Appendix A.

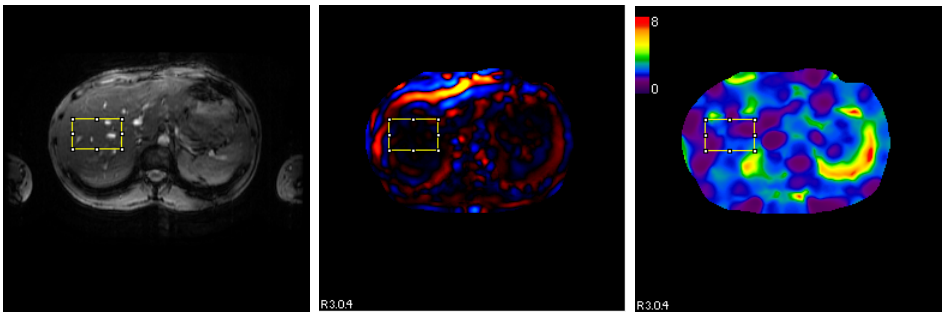

(a) Anatomy (b) Wave map (c) Shear stiffness (kPa)

Figure 6.1: MRE of a healthy individual. (a) Shows the anatomy and is the original MRE image. It shows a cross section of the body and the liver where the liver is located to the left. (b) Shows how the sinusoidal wavefront propagates through the body and the liver. (c) Shows the shear stiffness of the body in kPa, computed using the software MRE/Wave. The yellow boxes indicates the domain studied in the numerical work and is located inside the liver.

6.1 Experiments with MRE data from a healthy liver using the Poisson minimization model

In the followin experiments, consider the domain marked by the yellow boxes in Figure 6.1. This domain will be denoted by Ω. By using the Poisson model and the source code from the previous experiments described in Chapter 4, qualitative experiments will be performed to decide the displacement and the shear modulus in the chosen domain.

The processing of the MRE data is described in Figure 6.2. MRE images are given as .dcm-files. These files are then used to produce a .csv file by using the MRE/Wave software [11]. The .csv file contains a matrix of a coordinate system representing the displacement of each image pixel. A python script reads the .csv-file and calculates the displacement due to the MRE waves. The result is stored as a numpy array in a .npy-file. Another python script makes a DOLFIN Expression from the numpy array, and this Expression can be used as u_{MR} in the experiments in Chapter 4. The work of this thesis starts with creating the numpy array.

We solve the the Poisson minimization problem for harmonic elastography with pure Neumann conditions on the whole boundary, given in (2.17), with $t = 0$. In the experiments with manufactured solutions in this model, the assumption $\rho\omega^2 = 1$, was made. In the following experiments we use the frequency of the sinusoidal wave in the MRE measurements, which was $f = 60$ Hz, thus the angular frequency becomes $\omega = 2\pi f = 120\pi$ rad/s.

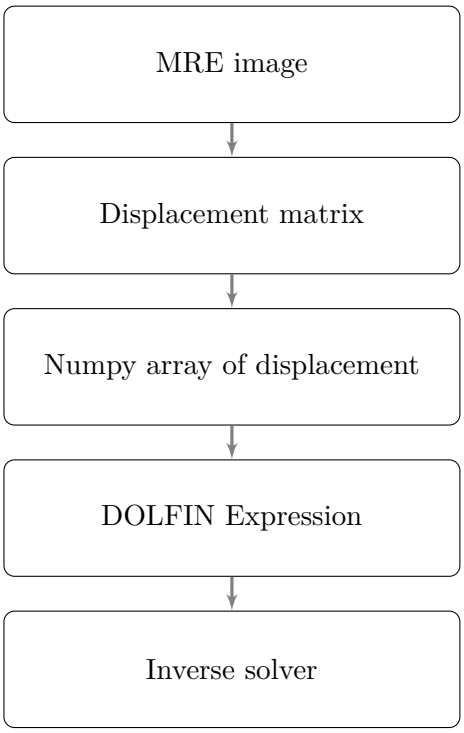

Figure 6.2: Processing of the MRE data.

Assume that the density of the body is $\rho = 1000$ kg/m^3, which is the density of water at body temperature. The target solution for the displacement, u_{MR} is the displacement calculated from the MRE data using the MRE/Wave software. For the chosen domain, Ω, the displacement is shown in Figure 6.3. A study performed by Rouviere et al. [31] found that the mean shear stiffness of healthy human livers were 2.0 kPa $\pm$ 0.3 kPa (standard deviation), thus this is used as a target solution for μ, that is $\mu_{\text{prior}} = 2000$ Pa.

We will in the rest of this chapter present 13 experiments with the liver MRE data and corresponding results. Unfortunately, the experiments were not successful and we did not manage to reconstruct the shear modulus field. In the description of these experiments, we argue why we do each of the modifications in each experiment. The modifications are based on the experience from the in-depth studies of the Poisson minimization problem, in Chapter 4, trying to improve the results. In almost all experiment setups, the obtained solution for the displacement field were approximately zero and the shear modulus field equals target solution for μ. We start by presenting the original setup for the experiments and the results obtained by this setup.

The following setup was used in the first experiment:

$$\alpha = 0.0$$
$$\mu_{\text{prior}} = 2000,$$

and the initial guesses in the Newton solver were (which are the same as in Chapter 4):

$$u_0 = u_{\text{MR}}$$
$$\mu_0 = \mu_{\text{prior}}$$
$$w_0 = 1.0,$$

with the following parameters in the Newton solver:

$$\text{maximum iterations} = 40$$
$$\text{absolute tolerance} = 10^{-10}$$
$$\text{relative tolerance} = 10^{-9}$$
$$\text{relaxation parameter} = 1.0.$$

The values for the absolute tolerance, relative tolerance and the relaxation parameter are all the default values in FEniCS.

Experiment 1 Figure 6.4 shows the computed solutions using this setup. The solutions to the left are for $\mu \in \mathbb{R}$ and the solutions to the right are for $\mu \in \text{DG}_0$. Ideally, u_{approx} should be similar to u_{MR} depicted in Figure 6.3, but comparing these figures it is clear that this is not the case. Also, μ_{approx} is expected to be similar to the marked area in Figure 6.1c, but this is not the case either. Evidently, using this setup does not provide good approximations.

Experiment 2 To obtain better approximations, a number of various modifications were made. First, we observe that the solution for the Lagrange multiplier w in experiment 1 is close to 0, this was also the case in the experiments with the Poisson model, described in Chapter 4. Thus, the modification

$$w_0 = 0.0 \tag{6.1}$$

is made. Solving the system with this modification provided the solutions shown in Figure 6.5. Secondly, we observe that the obtained solutions are different from the solutions in experiment 1. Without regularization the optimization problem is ill-posed and has non-unique solutions. With this setup, the Newton solver did not converge for heterogeneous shear modulus. We observe that the obtained approximation for the displacement is in the

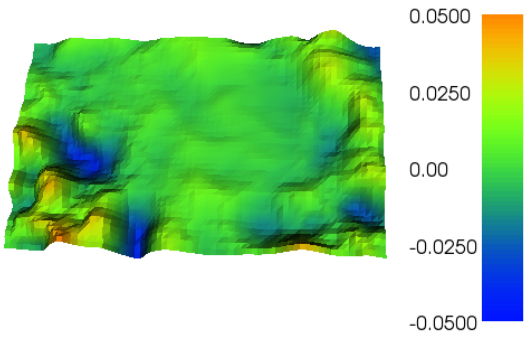

Figure 6.3: The displacement measured in meters computed from the MRE data which is the target solution, u_{MR}, in the experiments.

correct order of magnitude, but other than that, the solution does not correspond with the MR measurements. The approximation of μ is negative, which is not physically correct and therefore not a satisfactory solution.

Experiment 3 To make the problem well-posed, we add regularization. Let the regularization parameter $\alpha = 10^{-5}$, which was an optimal value in the previous experiments with the Poisson model. The resulting solutions are depicted in Figure 6.6. Observe that the solution of u in the homogeneous case has the same shape as u_{MR}, but unfortunately it is off by 12 orders of magnitude and is approximately zero. For the heterogeneous case, the shape similarity of the approximation of u and u_{MR} is a little less evident and it disagrees with u_{MR} with 10 orders of magnitude. In both these cases, the solution of μ is in the expected order of magnitude and the solution becomes constant.

Experiment 4 Since the previous setup gave solutions of the displacement field with the expected shape, but wrong order of magnitude, we consider more strict convergence criteria in the Newton solver. Let the absolute tolerance be 10^{-16} (machine precision) and let relative tolerance be 10^{-15}. The results from this setup are shown in Figure 6.7. Having stricter convergence criteria, we expected the computed displacement field to get closer to the measured field. However, the obtained solutions for both homogeneous and heterogeneous μ, were zero and even further away from the measured displacement than in the previous experiment. In both these cases μ_{approx} stays constant and equals the initial guess.

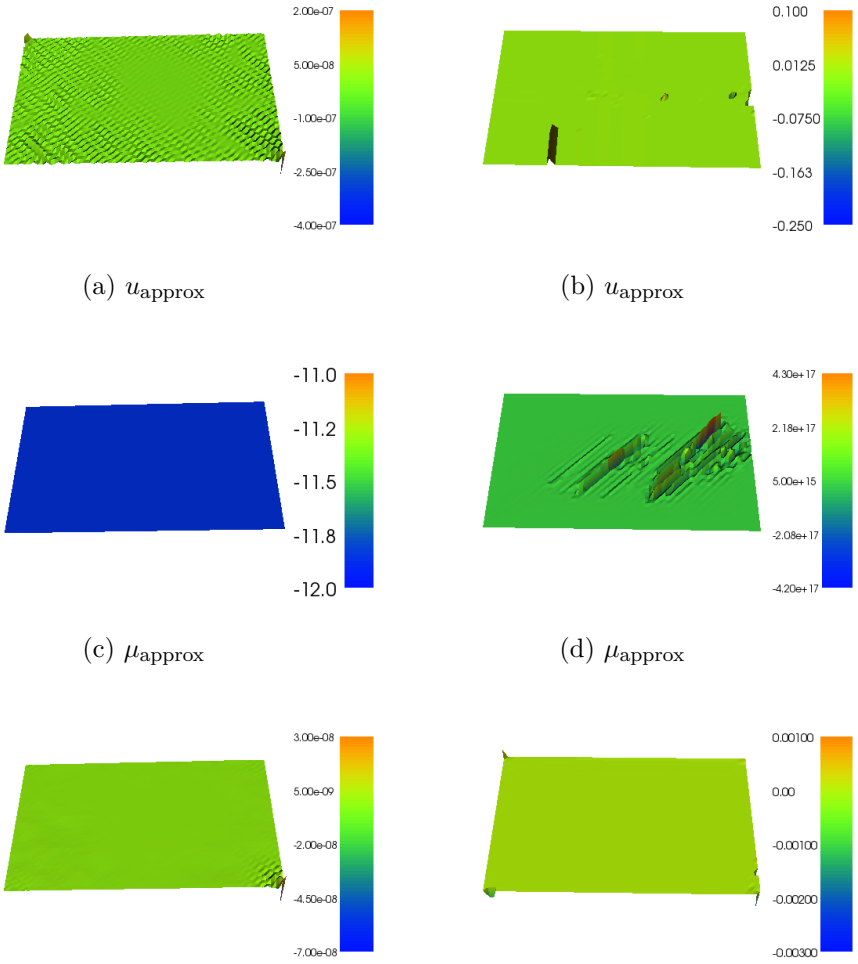

(a) u_{approx} (b) u_{approx}

(c) μ_{approx} (d) μ_{approx}

(e) w_{approx} (f) w_{approx}

Figure 6.4: Experiment 1: Solutions from experiments with the following setup: $\alpha = 0.0$. Neumann boundary conditions on the whole boundary: $\mu\frac{\partial u}{\partial \boldsymbol{n}} = 0$ on $\partial\Omega$. Target solution for μ: $\mu_{\text{prior}} = 2000$. Initial guesses: $u_0 = u_{\text{MR}}, \mu_0 = \mu_{\text{prior}}, w_0 = 1.0$. Parameters in Newton solver: maximum iterations = 40, absolute tolerance = 10^{-10}, relative tolerance = 10^{-9}, relaxation parameter = 0. In (a), (c) and (e) $\mu \in \mathbb{R}$ and in (b), (d) and (f) $\mu \in \text{DG}_0$.

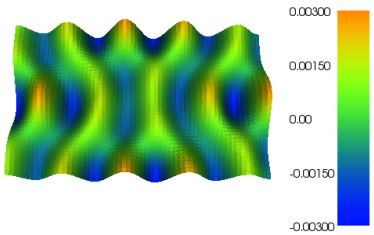

(a) u_{approx}

(b) μ_{approx}

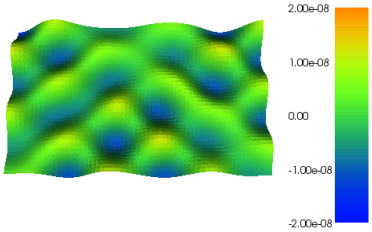

(c) w_{approx}

Figure 6.5: Experiment 2: Solutions from experiments with the following setup: $\alpha = 0.0$. Neumann boundary conditions on the whole boundary: $\mu\frac{\partial u}{\partial \boldsymbol{n}} = 0$ on $\partial\Omega$. Target solution for μ: $\mu_{\text{prior}} = 2000$. Initial guesses: $u_0 = u_{\text{MR}}, \mu_0 = \mu_{\text{prior}}, w_0 = 0.0$. Parameters in Newton solver: maximum iterations = 40, absolute tolerance = 10^{-10}, relative tolerance = 10^{-9}, relaxation parameter = 0. In (a), (c) and (e) $\mu \in \mathbb{R}$ and in (b), (d) and (f) $\mu \in \text{DG}_0$.

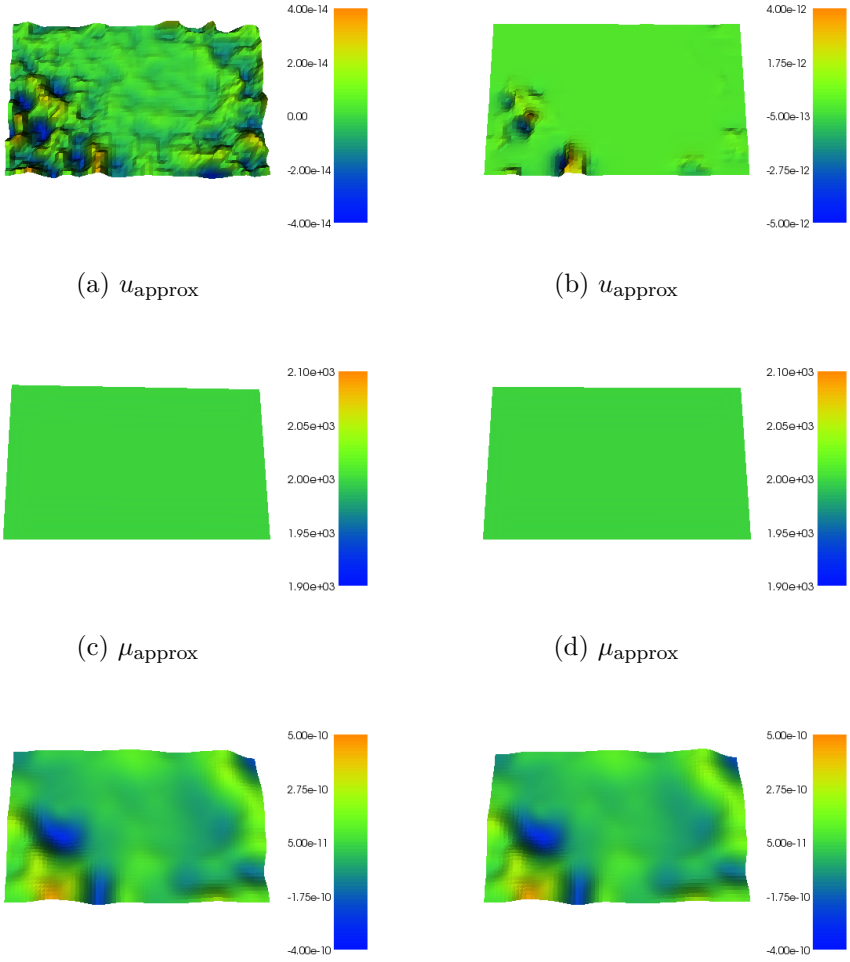

(a) u_{approx} (b) u_{approx}

(c) μ_{approx} (d) μ_{approx}

(e) w_{approx} (f) w_{approx}

Figure 6.6: Experiment 3: Solutions from experiments with the following setup: $\alpha = 10^{-5}$. Neumann boundary conditions on the whole boundary: $\mu\frac{\partial u}{\partial \boldsymbol{n}} = 0$ on $\partial\Omega$. Target solution for μ: $\mu_{\text{prior}} = 2000$. Initial guesses: $u_0 = u_{\text{MR}}, \mu_0 = \mu_{\text{prior}}, w_0 = 0.0$. Parameters in Newton solver: maximum iterations = 40, absolute tolerance = 10^{-10}, relative tolerance = 10^{-9}, relaxation parameter = 0. In (a), (c) and (e) $\mu \in \mathbb{R}$ and in (b), (d) and (f) $\mu \in \text{DG}_0$.

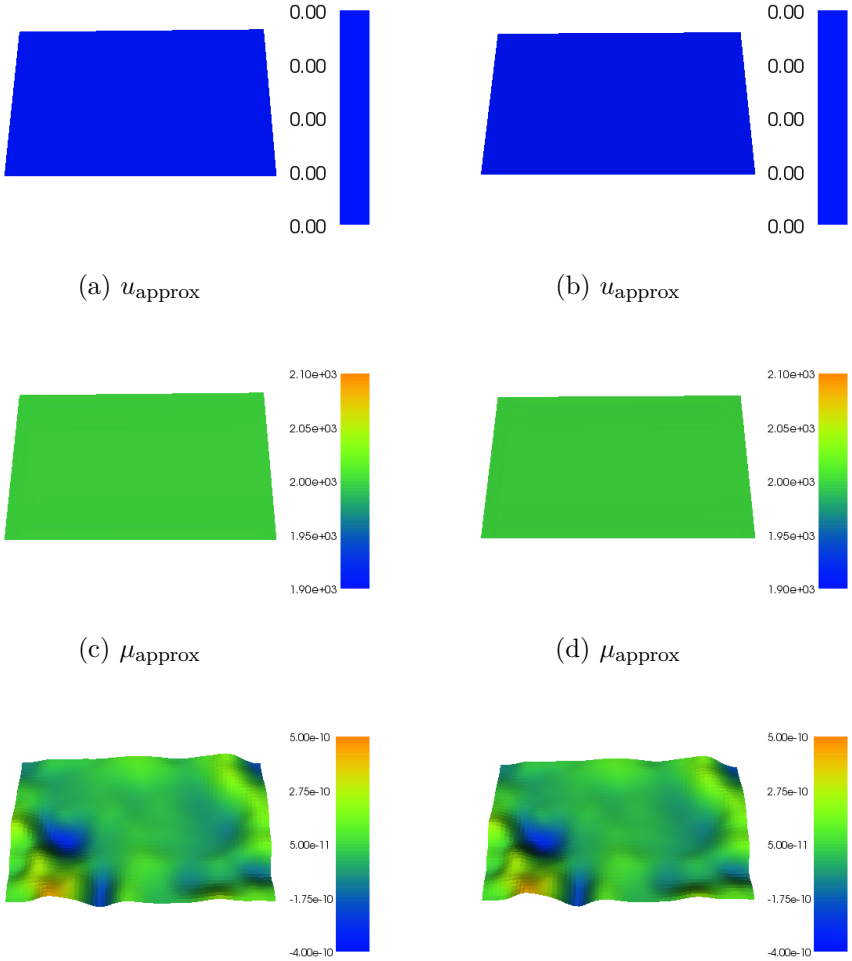

(a) u_{approx} (b) u_{approx}

(c) μ_{approx} (d) μ_{approx}

(e) w_{approx} (f) w_{approx}

Figure 6.7: Experiment 4: Solutions from experiments with the following setup: $\alpha = 10^{-5}$. Neumann boundary conditions on the whole boundary: $\mu\frac{\partial u}{\partial \boldsymbol{n}} = 0$ on $\partial\Omega$. Target solution for μ: $\mu_{\text{prior}} = 2000$. Initial guesses: $u_0 = u_{\text{MR}}, \mu_0 = \mu_{\text{prior}}, w_0 = 0.0$. Parameters in Newton solver: maximum iterations = 40, absolute tolerance = 10^{-16}, relative tolerance = 10^{-15}. In (a), (c) and (e) $\mu \in \mathbb{R}$ and in (b), (d) and (f) $\mu \in \text{DG}_0$.

Experiment 5 Having stricter convergence criteria did not yield satisfactory solutions either. Instead we try changing the relaxation parameter and again we let the convergence criteria be of the default values. To make smaller changes in the solutions of each iteration, let the relaxation parameter $\omega_{\text{rel}} = 0.5$. The results from this experiment are presented in Figure 6.8. We observe that these results are very similar to those in Figure 6.6. The exceptions are that in this case the solutions are equal for homogeneous and heterogeneous μ and u_{approx} are three orders of magnitude larger. The solutions for the Lagrange multipliers are equal.

Experiment 6 In all of the previous experiments the obtained solutions of μ have been constant, even if searching for a variable solution of μ, and the solutions are equal to the target guess. Thus, to obtain s solution closer to the measured solution we try letting μ_{prior} be a function in DG_0 with random integer values in each of the elements. The study performed by Rouviere et al. [31] found that the mean shear stiffness of healthy human livers are 2.0 $\pm$ 0.3 kPa. Therefore we let each cell in μ_{prior} be a random value between 1700 Pa and 2300 Pa. The resulting approximations are shown in Figure 6.9. Observe that the solutions for u and w are equal. For $\mu_{\text{approx}} \in \mathbb{R}$, the solution is 2 kPa and for $\mu_{\text{approx}} \in \text{DG}_0$, the solution is equal to the random valued target solution μ_{prior}. Thus, it seems like the choice of μ_{prior} is dominant, even though the regularization is weak.

Experiment 7 Because the target guess μ_{prior} appears to be a decisive factor in the solutions, a better target solution for μ may improve the solutions of the minimization problem. We use the Poisson equation for harmonic deformations,

$$\rho\omega u - \mu\Delta u = 0,$$

to calculate μ_{prior} by direct inversion:

$$\mu_{\text{prior}} = \frac{\rho\omega u}{\Delta u}. \tag{6.2}$$

In the implementation, this is calculated in discrete values by computing the mass matrix, M, and the stiffness matrix, A. These matrices are defined in the following way:

$$\begin{aligned} M &= \int_\Omega uv \,\mathrm{d}x, d \\ A &= \int_\Omega \nabla u \cdot \nabla v \,\mathrm{d}x.d \end{aligned} \tag{6.3}$$

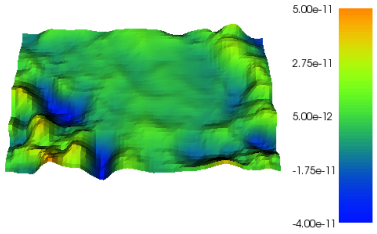

(a) u_{approx}

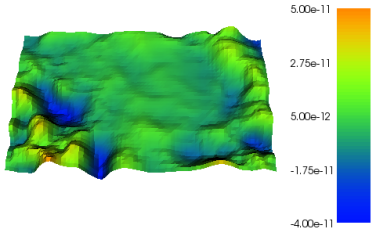

(b) u_{approx}

(c) μ_{approx}

(d) μ_{approx}

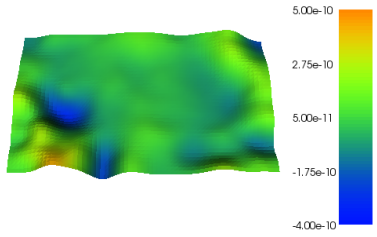

(e) w_{approx}

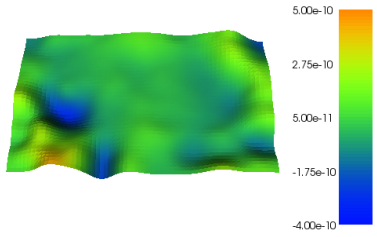

(f) w_{approx}

Figure 6.8: Experiment 5: Solutions from experiments with the following setup: $\alpha = 10^{-5}$. Neumann boundary conditions on the whole boundary: $\mu\frac{\partial u}{\partial \boldsymbol{n}} = 0$ on $\partial\Omega$. Target solution for μ: $\mu_{\text{prior}} = 2000$. Initial guesses: $u_0 = u_{\text{MR}}, \mu_0 = \mu_{\text{prior}}, w_0 = 0.0$. Parameters in Newton solver: maximum iterations = 40, absolute tolerance = 10^{-10}, relative tolerance = 10^{-9}, relaxation parameter to 0.5. In (a), (c) and (e) $\mu \in \mathbb{R}$ and in (b), (d) and (f) $\mu \in \text{DG}_0$.

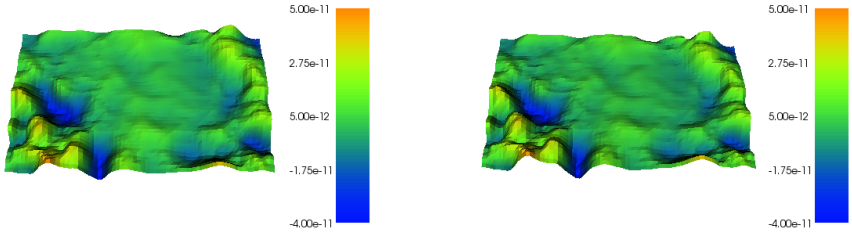

(a) u_{approx}

(b) u_{approx}

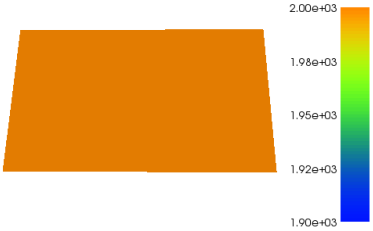

(c) μ_{approx}

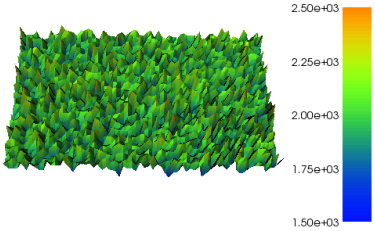

(d) μ_{approx}

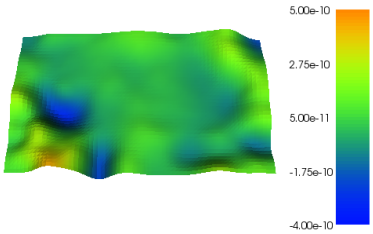

(e) w_{approx}

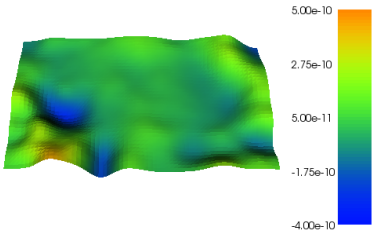

(f) w_{approx}

Figure 6.9: Experiment 6: Solutions from experiments with the following setup: $\alpha = 10^{-5}$. Neumann boundary conditions on the whole boundary: $\mu\frac{\partial u}{\partial \boldsymbol{n}} = 0$ on $\partial\Omega$. Target solution for μ:$\mu_{\text{prior}} = \text{randint}(1700, 2300)$. Initial guesses: $u_0 = u_{\text{MR}}, \mu_0 = \mu_{\text{prior}}, w_0 = 0.0$. Parameters in Newton solver: maximum iterations = 40, absolute tolerance = 10^{-10}, relative tolerance = 10^{-9}, relaxation parameter = 0.5. In (a), (c) and (e) $\mu \in \mathbb{R}$ and in (b), (d) and (f) $\mu \in \text{DG}_0$.

Here u is a trial function and v is a test function. Thus, the definition of μ_{prior} in the implementation is:

$$\mu_{\text{prior}} = \frac{\rho\omega M u_{\text{MR}}}{A u_{\text{MR}}}. \tag{6.4}$$

Solving the minimization problem with this setup yield the solutions depicted in Figure 6.10. In this case, the solutions of u are of about the expected orders of magnitude, but the shapes are not similar to the shape of u_{MR}. Also, μ is a lot larger than expected, and in the variable case it does not resemble the computed shear stiffness from MRE/Wave. To try to get better resemblance in μ, we tested searching for a continuous μ, that is $\mu \in \text{CG}_1$, however the Newton solver diverged.

Experiment 8 and 9 In the following experiment we consider other boundary conditions. Instead of $t = 0$ in the Neumann boundary conditions, let

$$t = \mu \frac{\partial u_{\text{MR}}}{\partial \boldsymbol{n}}, \tag{6.5}$$

where we let μ be the unknown parameter. The resulting approximations are shown in Figure 6.11. In this case u_{approx} is of the expected order of magnitude, however the shape of the field does not resemble the measured displacement field. The solution μ_{approx} becomes equal to the target solution $\mu_{\text{prior}} = 2000$, both when $\mu \in \mathbb{R}$ and $\mu \in \text{DG}_0$.

Letting $t = \mu_{\text{prior}} \frac{\partial u_{\text{MR}}}{\partial \boldsymbol{n}}$, yield the same results.

Experiment 10, 11 and 12 Now, consider Dirichlet boundary conditions instead of Neumann boundary conditions. Applying the Dirichlet boundary condition

$$u = u_{\text{MR}} \quad \text{on } \partial\Omega, \tag{6.6}$$

the Newton solver did not converge. Applying this conditions only on the left or the bottom boundary and $u = 0$ on the rest of the boundaries, did not yield convergence either. Thus, no results were obtained with Dirichlet boundary conditions.

Experiment 13 So far, none of the tested configurations have given satisfactory solutions. As a last attempt, consider changing the regularization parameter to try to obtain better solutions. The choice of the target guess for μ seems to be dominating the solving of the minimization problem, thus we let $\alpha = 10^{-6}$ instead of $\alpha = 10^{-5}$. Otherwise, let the setup be the same as in experiment 5. The resulting solutions from this new setup are presented in Figure 6.12. Comparison of these two figures show that the results

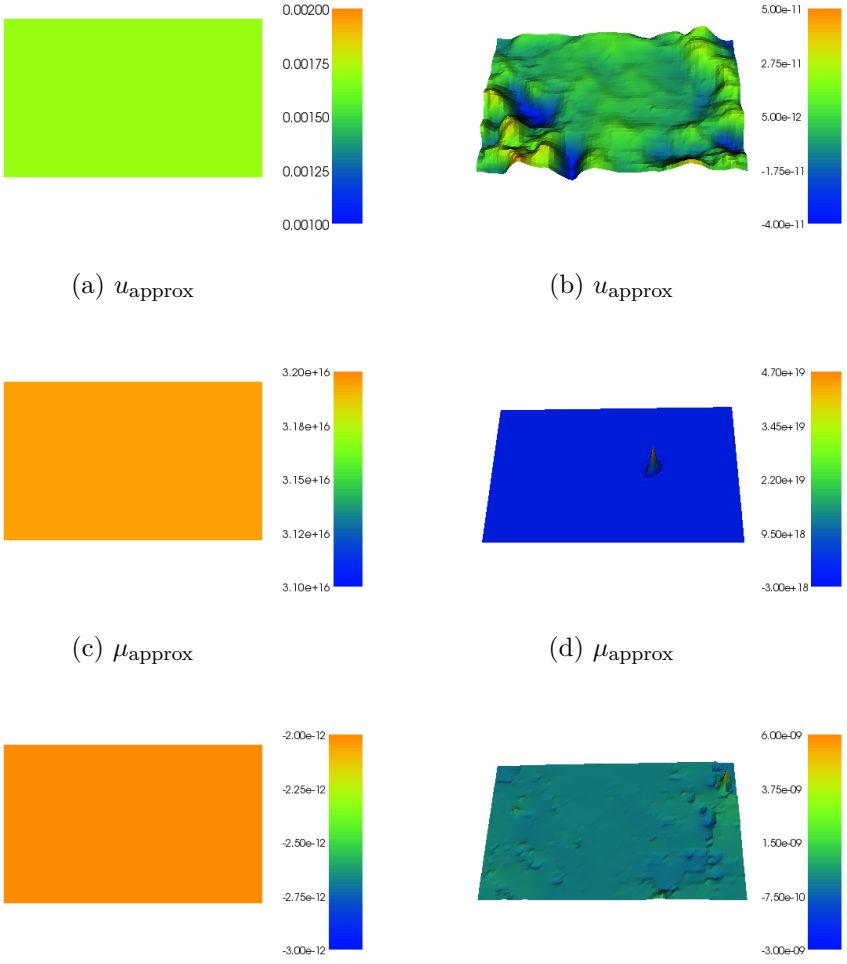

(a) u_{approx} (b) u_{approx}

(c) μ_{approx} (d) μ_{approx}

(e) w_{approx} (f) w_{approx}

Figure 6.10: Experiment 7: Solutions from experiments with the following setup: $\alpha = 10^{-5}$. Neumann boundary conditions on the whole boundary: $\mu\frac{\partial u}{\partial \boldsymbol{n}} = 0$ on $\partial\Omega$. Target solution for μ: $\mu_{\text{prior}} = \frac{\rho\omega^2 u_{\text{MR}}}{\Delta u_{\text{MR}}}$. Initial guesses: $u_0 = u_{\text{MR}}, \mu_0 = \mu_{\text{prior}}, w_0 = 0.0$. Parameters in Newton solver: maximum iterations = 40, absolute tolerance = 10^{-10}, relative tolerance = 10^{-9}, relaxation parameter = 0.5. In (a), (c) and (e) $\mu \in \mathbb{R}$ and in (b), (d) and (f) $\mu \in \text{DG}_0$.

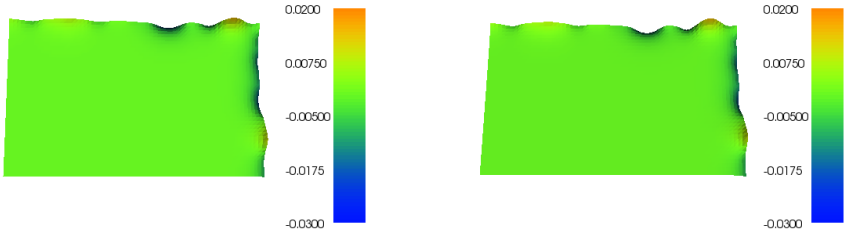

(a) u_{approx}

(b) u_{approx}

(c) μ_{approx}

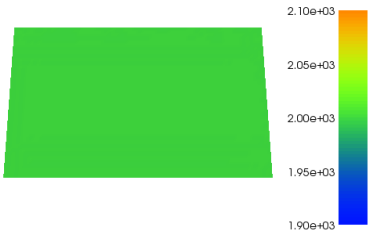

(d) μ_{approx}

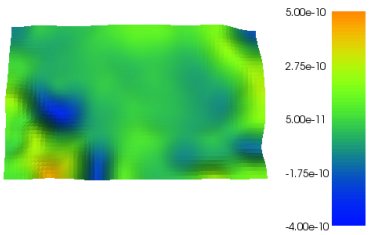

(e) w_{approx}

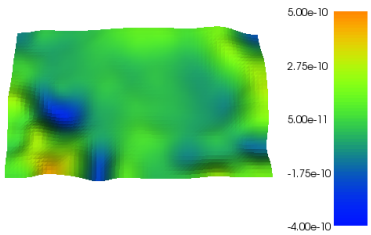

(f) w_{approx}

Figure 6.11: Experiment 8: Solutions from experiments with the following setup: $\alpha = 10^{-5}$. Neumann boundary conditions on the whole boundary: $\mu\frac{\partial u}{\partial \boldsymbol{n}} = t$ on $\partial\Omega$, where t is computed based on u_{MR} and μ is the function to solve for. Target solution for μ: $\mu_{\text{prior}} = 2000$. Initial guesses: $u_0 = u_{\text{MR}}, \mu_0 = \mu_{\text{prior}}, w_0 = 0.0$. Parameters in Newton solver: maximum iterations = 40, absolute tolerance = 10^{-10}, relative tolerance = 10^{-9}, relaxation parameter = 0.5. In (a), (c) and (e) $\mu \in \mathbb{R}$ and in (b), (d) and (f) $\mu \in \text{DG}_0$.

are approximately equal, and therefore making the regularization parameter smaller did not improve the results.

As seen from this review of the experiments with MRE data, we did not succeed in reconstructing the shear modulus of the liver using the one-shot optimization approach. We will discuss this further in the next chapter.

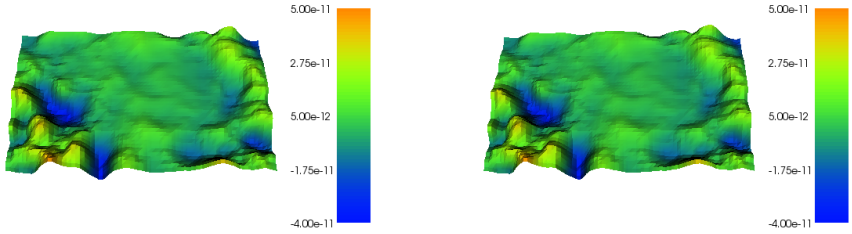

(a) u_{approx}

(b) u_{approx}

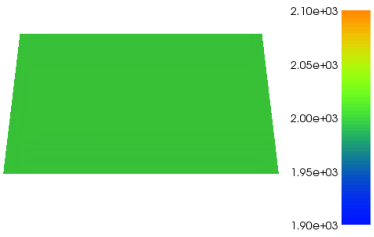

(c) μ_{approx}

(d) μ_{approx}

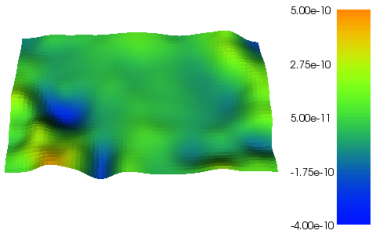

(e) w_{approx}

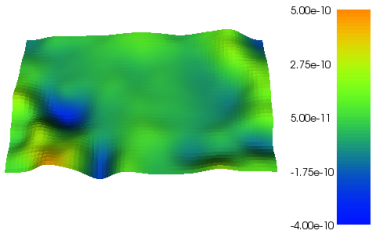

(f) w_{approx}

Figure 6.12: Experiment 13: Solutions from experiments with the following setup: $\alpha = 10^{-6}$. Neumann boundary conditions on the whole boundary: $\mu\frac{\partial u}{\partial \boldsymbol{n}} = 0$ on $\partial\Omega$. Target solution for μ: $\mu_{\text{prior}} = 2000$. Initial guesses: $u_0 = u_{\text{MR}}, \mu_0 = \mu_{\text{prior}}, w_0 = 0.0$. Parameters in Newton solver: maximum iterations = 40, absolute tolerance = 10^{-10}, relative tolerance = 10^{-9}, relaxation parameter to 0.5. In (a), (c) and (e) $\mu \in \mathbb{R}$ and in (b), (d) and (f) $\mu \in \text{DG}_0$.

Chapter 7

Discussion

In this thesis we have studied two models for describing harmonic deformation of biological tissue. These models are the Poisson equation and the linear elasticity model. To reconstruct the mechanical properties of tissue, we have solved PDE-constrained optimization problems by the one-shot approach. We have conducted in-depth studies of how Tikhonov regularization and noise in input data affects the solutions of these minimization problems with constructed data. Moreover, we have performed simulations with data from MRE examinations of a healthy liver in the Poisson optimization problem. By these experiments we tried to obtain the rheological properties of the liver.

Through the experiments with manufactured solutions it is clear that regularization is needed when the material is heterogeneous, that is, the material parameters (μ and λ) varies throughout the domain. With target solutions close to the exact solutions of the manufactured solutions, the one-shot approach yields qualitatively good results for both the displacement and the material parameters, both in the case of the Poisson problem and the linear elasticity problem. However, when simulating with the real MRE measurement data, the outcome was not as expected. Even though using the regularization that was found optimal in the case of the manufactured solution, the simulations did not yield satisfactory solutions.

The solutions we obtained in the simulations with real data were far from the target solutions. Therefore it is necessary to add more constraints in further experiments or reformulate the problem. Firstly, adding box constraints on u or μ (or both) may be a good approach. A box constraint restricts the solution with an upper and a lower bound, for instance:

$$\mu_{\min} \leq \mu \leq \mu_{\max}. \tag{7.1}$$

Applying such constraints will force the solution of μ to be within the set range.

In some of the experiments the solution of the displacement field was zero. By studying the optimization problem, this is obviously a solution to the PDE, however not a good solution to the minimization problem as it is far from the measured displacement field. When we get the solution $u = 0$, also the derivative of u is zero, and in that case all gradient-based optimization approaches will fail. A possible way to avoid this solution, is to add a constraint such that the displacement is not allowed to be zero everywhere. This can be done by adding a box constraint on the absolute value of u. Another possibility is to apply Dirichlet boundary conditions on parts of the boundary or on the whole boundary. Then the zero solution would no longer satisfy the constraints.

In the simulations with manufactured solutions, we did not test with an actual varying shear modulus field. Even though searching for a solution of μ varying throughout the domain, the exact solution of μ in the manufactured solutions was constant. Testing with a heterogeneous shear modulus in the manufactured solutions should therefore be investigated further.

In the experiments with manufactured solutions we used $\rho\omega^2 = 1$. However, in the experiments with real data the parameters are $\rho = 1000$ and $\omega = 120\pi$. Moreover, the value of μ in the manufactured solution of the Poisson problem was $\mu = 0.25$, whereas the expected value of the shear modulus of the liver is about 2000 Pa. It is uncertain how this difference in values affect the results, therefore it should be tested further.

7.1 Concurrence with other studies

A study by Oberai et al. [10] uses the one-shot approach to solve the quasi-static inverse elasticity model with constructed data. This study yielded similar results as the experiments with manufactured solutions in this thesis. Yuan and Guzina [32] successfully applied an adjoint-based approach to reconstruct the viscoelastic tissue properties. However, also in this study only constructed data were considered. The most commonly used method to reconstruct material parameters and create elastograms are direct inversion schemes [15]. This have been done in the following studies [14; 33]. However, when solving with a direct scheme the results are less accurate than for a gradient-based approach such as the one-shot approach [15].

7.2 Conclusion

We have successfully implemented inverse solvers for both the Poisson and the linear elasticity minimization problems. By using manufactured solutions we have been able to reconstruct the displacement field and the material parameters in the optimization problems. Even with up to 10 % of synthetic noise in the target solution of the displacement field, the obtained solutions of the minimization problem were qualitatively good when Tikhonov regularization were added and/or prior knowledge of the material parameters were used.

However, when solving the inverse Poisson problem with data from MRE measurements, the method failed. The obtained results in these simulations were far from the measured solutions. Even though these solutions satisfied the minimization problem, they are not satisfactory solutions, as they fails in reconstructing the measured data. For this method to have potential more constraints must be added, other boundary conditions must be applied or the optimization problem must be defined differently.

To my knowledge the one-shot optimization method has not been used to reconstruct material properties of tissue with real MRE data in previous research. In all publications I have found, this method has only been tested with constructed data. Also, to my knowledge all successful reconstructions of the rheological parameters of biological tissue are conducted using other inversion methods, such as direct inversion schemes.

7.3 Future work

The results of this thesis shows that the one-shot optimization approach yields qualitatively good results in the simulations with constructed data. However, in simulations with real MRE data the method fails to give satisfactory solutions. Therefore future work should involve further investigations of the method with manufactured solutions, such as

- test with manufactured solutions closer to the values of the MRE data in both the Poisson and the linear elasticity models, and
- test with heterogeneous parameters in the manufactured solutions for both models.

Moreover, in the experiments with real MRE data the following modifications should be investigated:

- adding more constraints, for instance box constraints such as

$$\mu_{\min} \leq \mu \leq \mu_{\max}$$

or

$$u_{\min} \leq |u| \leq u_{\max},$$

and

- other boundary conditions.

If none of these suggestions succeed in obtaining qualitatively good solutions to the optimization problems, the optimization problems should be defined differently or other approaches should be considered.

Appendix A

Source code

A.1 Solver for the Poisson optimization problem

```
from dolfin import *
import ufl, sys, random, numpy
from time import clock, strftime, gmtime

def convergence_rate(E, h):
    from math import log as ln
    r = []
    for i in range(1, len(E)):
        if E[i] and E[i-1]:
            r.append(ln(E[i]/E[i-1])/ln(h[i]/h[i-1]))
        else:
            r.append("False")
    return r

def solver(N, k, noise, degree=1, makeplot=False, alpha=0.0, mu_space="constant",
                                                            mu_prior_function="0"):
    # Create mesh
    mesh = UnitSquareMesh(N, N)

    # Create classes for defining parts of the boundaries
    class Left(SubDomain):
        def inside(self, x, on_boundary):
            return near(x[0], 0.0)
    class Right(SubDomain):
        def inside(self, x, on_boundary):
            return near(x[0], 1.0)
    class Bottom(SubDomain):
        def inside(self, x, on_boundary):
            return near(x[1], 0.0)
    class Top(SubDomain):
        def inside(self, x, on_boundary):
            return near(x[1], 1.0)

    # Initialize sub-domain instances
    left = Left()
    top = Top()
    right = Right()
```

```
bottom = Bottom()

V = FunctionSpace(mesh, 'Lagrange', degree)
if mu_space == "constant":
    S = FunctionSpace(mesh, 'R', 0)
elif mu_space == "DG":
    S = FunctionSpace(mesh, 'DG', 0)

M = MixedFunctionSpace([V, S, V])

# Code for C++ evaluation of noise function
noise_code = """
class Noise : public Expression
{
public:
  // Create expression
  Noise() : Expression() {}

  // Function for evaluating expression on each cell
  void eval(Array<double>& values, const Array<double>& x,
                                                const ufc::cell& cell) const
  {
    const uint D = cell.topological_dimension;
    const uint cell_index = cell.index;
    values[0] = (*noise_mesh)[cell_index];
  }

  // The data stored in mesh functions
  boost::shared_ptr<MeshFunction<double> > noise_mesh;
};
"""

# Define known functions
u_exact = Expression('exp(-k*x[0])', k = k, degree = degree)
mu_exact = Expression('1.0/(k*k)', k = k, degree = degree)

if noise != 0.0:
    # Define noise expression
    noise_mesh = MeshFunction("double", mesh,
                              "noise/u_MR_mesh_noise_%s_N_%i.xml.gz" % (noise, N))
    noise_function = Expression(cppcode=noise_code)
    noise_function.noise_mesh = noise_mesh
    u_MR = u_exact + noise_function
else:
    u_MR = u_exact

if mu_prior_function == "0":
    mu_prior = Constant(0.0)
elif mu_prior_function == "mu_exact":
    mu_prior = mu_exact

print "-----------------------------------------------------------------"
print "Computing solution. mu_prior = %s,  alpha = %s, noise = %s, N = %i,
                                                        degree = %i \n" \
        % (mu_prior_function, alpha, noise, N, degree)

# Define trial functions and test functions
z = TestFunction(M)
(v, eta, q) = split(z)

# Define function
y = Function(M)
```

```
# Set initial guesses
u0  = u_exact
mu0 = mu_exact
w0  = Expression("1.0")

y0 = project(as_vector((u0, mu0, w0)), M)
y.assign(y0)

# Split mixed functions
(u, mu, w) = split(y)

# Initialize mesh function for boundary domains
boundaries = FacetFunction("size_t", mesh)
left.mark(boundaries, 0)
top.mark(boundaries, 2)
right.mark(boundaries, 1)
bottom.mark(boundaries, 2)

# Define boundary conditions
t_l = Constant(1.0/k)
t_r = Constant(-exp(-k)/k)
n = FacetNormal(mesh)
t = dot(project(mu_exact, S)*grad(project(u_exact, V)), n)

# Define new measures associated with the boundaries
ds = Measure("ds")[boundaries]

# Define Lagrangian
L = (u - u_MR)**2*dx + u*w*dx \
    + inner(mu*grad(u), grad(w))*dx \
    + alpha*(mu - mu_prior)**2*dx \
    - t_l*w*ds(0) - t_r*w*ds(1)

# Compute directional derivatives
F = derivative(L, y, z)

# Solve nonlinear problem
problem = NonlinearVariationalProblem(F, y, J=derivative(F, y))
newtonsolver = NonlinearVariationalSolver(problem)
max_iter = 40
newtonsolver.parameters["newton_solver"]["maximum_iterations"] = max_iter
newtonsolver.parameters["newton_solver"]["absolute_tolerance"] = 1E-13
newtonsolver.parameters["newton_solver"]["relative_tolerance"] = 1E-12
start = clock()
try:
    iterations, convergence = newtonsolver.solve()
except RuntimeError:
    iterations = max_iter
    convergence = False
end = clock()
print "finished solving"

# Plot solution
if makeplot:
    plot(mesh)
    u_V = project(u, V)
    u_e_V = project(u_exact, V)
    u_MR_V = project(u_MR, V)
    mu_S = project(mu, S)
    w_V = project(w, V)
    plot(u_V, title="Numerical solution of u, N=%i, alpha=%s, noise=%s,
```

```
                                        mu_space=%s" % (N, alpha, noise, mu_space))
        plot(u_e_V, title="Analytical solution of u, N=%i, alpha=%s, noise=%s,
                                        mu_space=%s" % (N, alpha, noise, mu_space))
        plot(u_MR_V, title="u_MR, N=%i, alpha=%s, noise=%s, mu_space=%s"
                                                    % (N, alpha, noise, mu_space))
        plot(mu_S, title="numerical solution of mu, N=%i, alpha=%s, noise=%s,
                                        mu_space=%s" % (N, alpha, noise, mu_space))
        plot(w_V, title="Numerical solution of w, N=%i, alpha=%s, noise=%s,
                                        mu_space=%s" % (N, alpha, noise, mu_space))
        interactive()

    if convergence:

        # Compute error in u
        (u, mu, w) = y.split(True)

        u_exact = Expression('exp(-k*x[0])', k = k, degree = degree + 4)
        mu_exact = Expression('1.0/(k*k)', k = k, degree = degree + 4)

        error_u_L2    = errornorm(u_exact, u, 'L2')
        error_u_H1    = errornorm(u_exact, u, 'H1')
        error_mu_L2   = errornorm(mu_exact, mu, 'L2')
        mu_approx_avg = numpy.mean(mu.vector().array())
        mu_std        = numpy.std(mu.vector().array())
        mu_e_vector   = numpy.ones(len(mu.vector().array()))*(1.0/k**2)
        diff          = mu.vector().array() - numpy.ones(len(mu.vector().array()))
                                                                    *mu_approx_avg
        mu_dev        = numpy.abs(diff).max()

        print "\nerror_u (L2-norm): ", error_u_L2
        print "error_u (H1-norm): ", error_u_H1
        print "mu_error (L2-norm): ", error_mu_L2
        print "mu average: %.4f" % mu_approx_avg
        print "mu std    : %.4f" % mu_std
        print "mu max dev: %.4f" % mu_dev

        return error_u_L2, error_u_H1, error_mu_L2, end - start, iterations,
                                                    mu_approx_avg, mu_std, mu_dev
    else:
        return False, False, False, end - start, max_iter, False, False, False


N = 32
k = 2.0
noise = 0.0        # 0.0, 0.003, 0.01, 0.03, 0.1
degree = 1
makeplot = True
alpha = 0.0
mu_space = "constant" # "constant" or "DG"
mu_prior_function = "0" # "0" or "mu_exact"
solver(N, k, noise, degree, makeplot, alpha, mu_space, mu_prior_function)
```

A.2 Script to generate synthetic noise in the Poisson problem

```
from dolfin import *
import random

noise_list = [0.003, 0.01, 0.03, 0.1]
N_list = [4, 8, 16, 32, 64, 128]
for N in N_list:
    print "Creating noise, N=%i" % N
    mesh = UnitSquareMesh(N, N)
    V = FunctionSpace(mesh, "CG", 1)
    for noise in noise_list:
        u_exact = Expression('exp(-k*x[0])', k = 2.0, degree = 1)
        u_exact_V = project(u_exact, V)

        u_MR_mesh = MeshFunction("double", mesh, 2)

        for cell in cells(mesh):
            u_MR_mesh[cell] = random.gauss(0, noise)*norm(u_exact_V, 'L2')

        u_MR_mesh_file = File("noise/u_MR_mesh_noise_%s_N_%i.xml.gz"% (noise, N))
        u_MR_mesh_file << u_MR_mesh

        plot(mesh, title="mesh")
        plot(u_MR_mesh, title="noise_%s_N_%i" % (noise, N))
```

Bibliography

[1] F. A. Duck. *Physical properties of tissue: a comprehensive reference book*. Academic Press, 1990.

[2] Y. K. Mariappan, K. J. Glaser, and R. L. Ehman. Magnetic resonance elastography: a review. *Clinical anatomy*, 23(5):497–511, 2010.

[3] J. F. Greenleaf, M. Fatemi, and M. Insana. Selected methods for imaging elastic properties of biological tissues. *Annual review of biomedical engineering*, 5(1):57–78, 2003.

[4] S. Cheng, E. C. Clarke, and L. E. Bilston. Rheological properties of the tissues of the central nervous system: a review. *Medical engineering & physics*, 30(10):1318–1337, 2008.

[5] M. Yin, J. Chen, K. J. Glaser, J. A. Talwalkar, and R. L. Ehman. Abdominal mr elastography. *Topics in magnetic resonance imaging: TMRI*, 20(2):79–87, 2009.

[6] D. C. Rockey, S. H. Caldwell, Z. D. Goodman, R. C. Nelson, and A. D. Smith. Liver biopsy. *Hepatology*, 49(3):1017–1044, 2009.

[7] M. Yin, J. A. Talwalkar, K. J. Glaser, A. Manduca, R. C. Grimm, P. J. Rossman, J. L. Fidler, and R. L. Ehman. Assessment of hepatic fibrosis with magnetic resonance elastography. *Clinical Gastroenterology and Hepatology*, 5(10):1207–1213, 2007.

[8] J. Foucher, E. Chanteloup, J. Vergniol, L. Castera, B. Le Bail, X. Adhoute, J. Bertet, P. Couzigou, and V. de Ledinghen. Diagnosis of cirrhosis by transient elastography (fibroscan): a prospective study. *Gut*, 55(3):403–408, 2006.

[9] K. R. Raghavan and A. E. Yagle. Forward and inverse problems in elasticity imaging of soft tissues. *Nuclear Science, IEEE Transactions on*, 41(4):1639–1648, 1994.

[10] A. A. Oberai, N. H. Gokhale, and G. R. Feijoo. Solution of inverse prob-

lems in elasticity imaging using the adjoint method. *Inverse Problems*, 19(2):297–313, 2003.

[11] Mayo clinic. `http://www.mayo.edu/research/labs/magnetic-resonance-imaging/mre-wave`.

[12] A. Logg, K.-A. Mardal, G. N. Wells, et al. *Automated Solution of Differential Equations by the Finite Element Method*. Springer, 2012. ISBN 978-3-642-23098-1. doi: 10.1007/978-3-642-23099-8.

[13] FEniCS Project. `http://www.fenicsproject.org/`, .

[14] A. Manduca, T. E. Oliphant, M. A. Dresner, J. L. Mahowald, S. A. Kruse, E. Amromin, J. P. Felmlee, J. F. Greenleaf, and R. L. Ehman. Magnetic resonance elastography: non-invasive mapping of tissue elasticity. *Medical image analysis*, 5(4):237–254, 2001.

[15] M. M. Doyley. Model-based elastography: a survey of approaches to the inverse elasticity problem. *Physics in medicine and biology*, 57(3): R35–R73, 2012.

[16] A. Kolipaka, K. P. McGee, A. Manduca, A. J. Romano, K. J. Glaser, Philip A. Araoz, and R. L. Ehman. Magnetic resonance elastography: Inversions in bounded media. *Magnetic Resonance in Medicine*, 62(6): 1533–1542, 2009.

[17] K. Atkinson and W. Han. *Theoretical Numerical Analysis*. Springer, third edition, 2009.

[18] D. Braess. *Finite Elements: Theory, Fast Solvers, and Applications in Solid Mechanics*. Cambridge University Press, Cambridge, third edition, 2007.

[19] S. W. Funke and P. E. Farell. A framwork for automated pde-constrained optimisation. *CoRR*, abs/1302.3894, 2013.

[20] A. Quarteroni. *Numerical Models for Differential Problems*, volume 2. Springer, 2009.

[21] M. S. Alnaes, A. Logg, K. B. Oelgaard, M. E. Rognes, and G. N. Wells. Unified form language: A domain-specific language for weak formulations of partial differential equations. *ACM Transactions on Mathematical Software, To appear, arXiv:1211.4047*, 2014.

[22] L. C. Evans. *Partial Differential Equations*. American Mathematical Society, second edition, 1998.

[23] C. Vogel. *Computational Methods for Inverse Problems*, volume 23 of *Frontiers in Applied Mathematics*. SIAM, 2002.

[24] S. Sheela and A. Singh. Tikhonov regularization of an elliptic pde. *Mathematics and computers in simulation*, 57(1):1–4, 2001.

[25] M. Hinze, R. Pinnau, M. Ulbrich, and S. Ulbrich. *Optimization with PDE Constraints*, volume 23 of *Mathematical Modelling: Theory and Applications*. Springer, 2009.

[26] H. P. Langtangen. *Computational partial differential equations: numerical methods and diffpack programming*. Springer, second edition, 2003. ISBN 978-3540434160.

[27] R. C. Kirby and A. Logg. *The finite element method*, chapter 2. Springer, 2012. ISBN 978-3-642-23098-1.

[28] S. C. Brenner and L. R. Scott. *Numerical methods in scientific computing*. Springer, New York, third edition, 2008.

[29] G. Dahlquist and Å. Björck. *The Mathematical Theory of Finite Element Methods*. SIAM, 2008.

[30] FEniCS tutorial (Python). `http://fenicsproject.org/documentation/tutorial/`, .

[31] O. Rouviere, M. Yin, M. A. Dresner, P. J. Rossman, L. J. Burgart, J. L. Fidler, and R. L. Ehman. Mr elastography of the liver: preliminary results. *Radiology-Radiological Society of North America*, 240(2):440–448, 2006.

[32] H. Yuan and B. B. Guzina. Reconstruction of viscoelastic tissue properties from mr elastography-type measurements. *Comptes Rendus Mecanique*, 338(7):480–488, 2010.

[33] R. Sinkus, J. Lorenzen, D. Schrader, M. Lorenzen, M. Dargatz, and D. Holz. High-resolution tensor mr elastography for breast tumour detection. *Physics in medicine and biology*, 45(6):1649, 2000.